Nano Research 2015, 8(2): 355–381
DOI 10.1007/s12274-014-0644-3
Review Article
ISSN 1998-0124
CN 11-5974/O4

The photoluminescence mechanism in carbon dots (graphene quantum dots, carbon nanodots, and polymer dots): Current state and future perspective

Shoujun Zhu, Yubin Song, Xiaohuan Zhao, Jieren Shao, Junhu Zhang, and Bai Yang (✉)

State Key Laboratory of Supramolecular Structure and Materials, College of Chemistry, Jilin University, Changchun 130012, P. R. China

Received: 9 September 2014
Revised: 10 November 2014
Accepted: 14 November 2014

KEYWORDS
carbon dots,
graphene quantum dots,
carbon nanodots,
polymer dots,
photoluminescence mechanism

ABSTRACT

At present, the actual mechanism of the photoluminescence (PL) of fluorescent carbon dots (CDs) is still an open debate among researchers. Because of the variety of CDs, it is highly important to summarize the PL mechanism for these kinds of carbon materials; doing so can guide the development of effective synthesis routes and novel applications. This review will focus on the PL mechanism of CDs. Three types of fluorescent CDs were involved: graphene quantum dots (GQDs), carbon nanodots (CNDs), and polymer dots (PDs). Four reasonable PL mechanisms have been confirmed: the quantum confinement effect or conjugated π-domains, which are determined by the carbon core; the surface state, which is determined by hybridization of the carbon backbone and the connected chemical groups; the molecule state, which is determined solely by the fluorescent molecules connected on the surface or interior of the CDs; and the crosslink-enhanced emission (CEE) effect. To give a thorough summary, the category and synthesis routes, as well as the chemical/physical properties for the CDs, are briefly introduced in advance.

1 Introduction

Carbon materials, which include graphite, diamond, fullerenes, carbon nanotubes (CNTs), and graphene, have been well known for many years. To make these materials fluorescent, their size and surface chemical groups should be carefully modulated. As-prepared fluorescent carbon materials always consist of sp^2/sp^3 carbon, oxygen/nitrogen-based groups, and post-modified chemical groups. Up to now, many kinds of fluorescent carbon-based nanomaterials have been synthesized, including carbon nanodots (CNDs) [1, 2], fluorescent carbon nanotubes (CNTs) [3], graphene oxide (GO) [4, 5], graphene quantum dots (GQDs) [6–12], polymer dots (PDs) [13–15], nanodiamonds [16, 17], and so on. In this review, carbon dots (CDs)—which include GQDs, CNDs, and PDs—prepared by chemical synthetic strategies are discussed. These three types of CDs possess similar photoluminescence (PL), although they are distinguished by their intrinsic

Address correspondence to byangchem@jlu.edu.cn

inner structure and surface chemical groups. The synthesis of CDs can be divided into top-down nano-cutting methods and bottom-up organic approaches. Top-down nano-cutting generally includes cutting different carbon resources such as GO, carbon fiber, CNTs, fullerenes, and graphite electrodes. Bottom-up organic approaches include carbonization of carbohydrates, self-assembly of polycyclic aromatic hydrocarbons (PAHs), and organic synthesis from small molecules.

At present, the actual mechanism of CD photoluminescence is still an open debate among researchers [18]. Because of the variety of CDs, it is highly important to summarize the PL mechanism for these types of carbon materials; doing so can guide the development of effective synthesis routes and novel applications. This review will therefore focus on the PL mechanism of CDs. Three types of fluorescent CDs are discussed: graphene quantum dots (GQDs), carbon nanodots (CNDs), and polymer dots (PDs) (Fig. 1) [19]. Four respectable PL mechanisms have been confirmed: the quantum confinement effect or conjugated π-domains, which are determined by the carbon core; the surface state, which is determined by hybridization of the carbon backbone and connected chemical groups; the molecule state, which is determined solely by the fluorescent molecules connected on the surface or interior of the CDs; and the crosslink-enhanced emission (CEE) effect. To give a thorough summary, the category, synthesis routes, and chemical/physical properties for CDs are briefly introduced in advance. Owing to the number of reports about CDs, we apologize to researchers whose important publications may be left out.

2 Category and synthesis routes

2.1 Classification of reported CDs

"CDs" is a comprehensive term for various nanosized carbon materials. In a broad sense, all nanosized materials that are composed mainly of carbon can be called CDs. CDs always possess at least one dimension less than 10 nm in size and fluorescence as their instinct properties. The structure of CDs consists of sp^2/sp^3 carbon and oxygen/nitrogen-based groups or polymeric aggregations. CDs mainly include GQDs, CNDs, and PDs (Fig. 1). GQDs possess one or a few layers of graphene and connected chemical groups on the edges. They are anisotropic with lateral dimensions larger than their height. CNDs are always spherical and they are divided into carbon nanoparticles, which

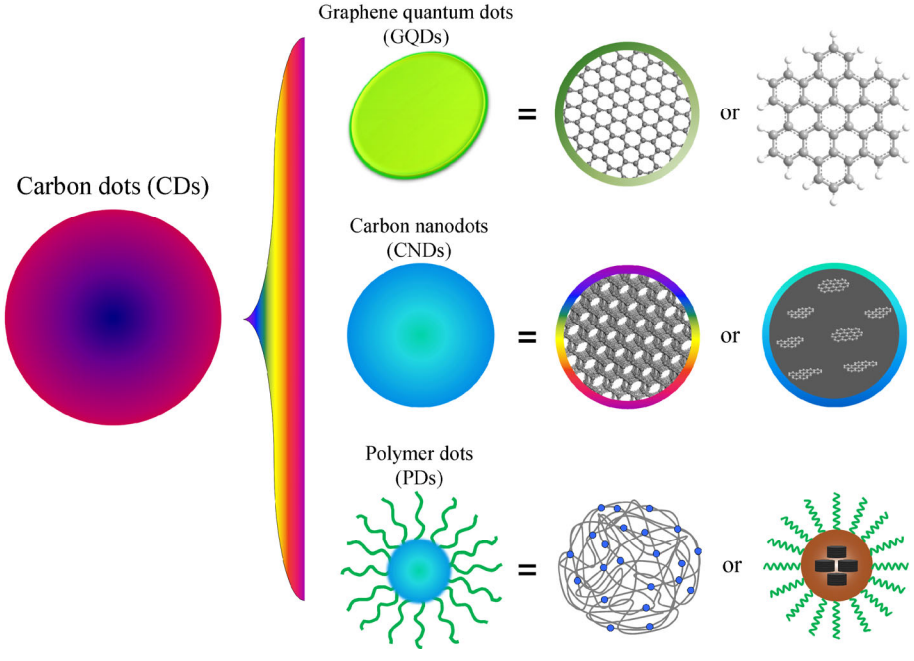

Figure 1 Three types of fluorescent CDs are discussed in this review: graphene quantum dots (GQDs), carbon nanodots (CNDs), and polymer dots (PDs).

do not have a crystal lattice, and carbon quantum dots (CQDs), which have an obvious crystal lattice. As a result, the PL center is very different for the different types of CNDs. PDs are aggregated or cross-linked polymers prepared from linear polymers or monomers. In addition, the carbon core and the connected polymer chains can self-assemble to form PDs. Owing to the diversity of CDs, there are many approaches to fabricating them, the most common of which are "top-down" cutting from different carbon sources and "bottom-up" synthesis from organic molecules or polymers and modification of surface functionality or passivation. We call the "top-down" and "bottom-up" routes "nano-methods," which are distinguished from the exclusively organic routes [20, 21].

2.2 "Top-down" cutting from different carbon sources

Generally, CDs are obtained by oxide cutting carbon resources such as graphite power [22], carbon rods [23], carbon fibers [24], carbon nanotubes [25, 26], carbon black [27], and even candle soot [28] (Fig. 2). These carbon materials possess a perfect sp^2 carbon structure and lack an efficient band gap to give fluorescence. To make these types of carbon sources photoluminescent, their size and surface chemistry must be carefully modulated. The most common cutting method uses a concentrated oxidizing acid (HNO_3 or an H_2SO_4/HNO_3 mixture) [29]. In this process, the bulk carbon materials are cut into small pieces and the surfaces of the pieces are modified by oxygen-based groups. The resulting small carbon product is known as GQDs, CQDs, or CNDs. It should be noted that two-step cutting routes have always been used to prepare GQDs. The first step is to convert a graphite-based material into GO sheets (usually using the modified Hummers method). The second step is cutting the GO into GQDs using various methods [30, 31].

Other "top-down" cutting routes include electrochemistry [32, 33], hydrothermal/solvothermal/special oxidation [30, 34], metal–graphite intercalation [35], and strong physical routes, such as arc discharge [36], laser ablation [37], and nanolithography by reactive ion etching (RIE) [38, 39]. In the electrochemistry method, the graphite rod electrode is broken up during the electrochemical cutting process to form CQDs or GQDs. The applied electrolyte contains ethanol [23], an ionic liquid [32], NaH_2PO_4 [40], tetrabutylammonium

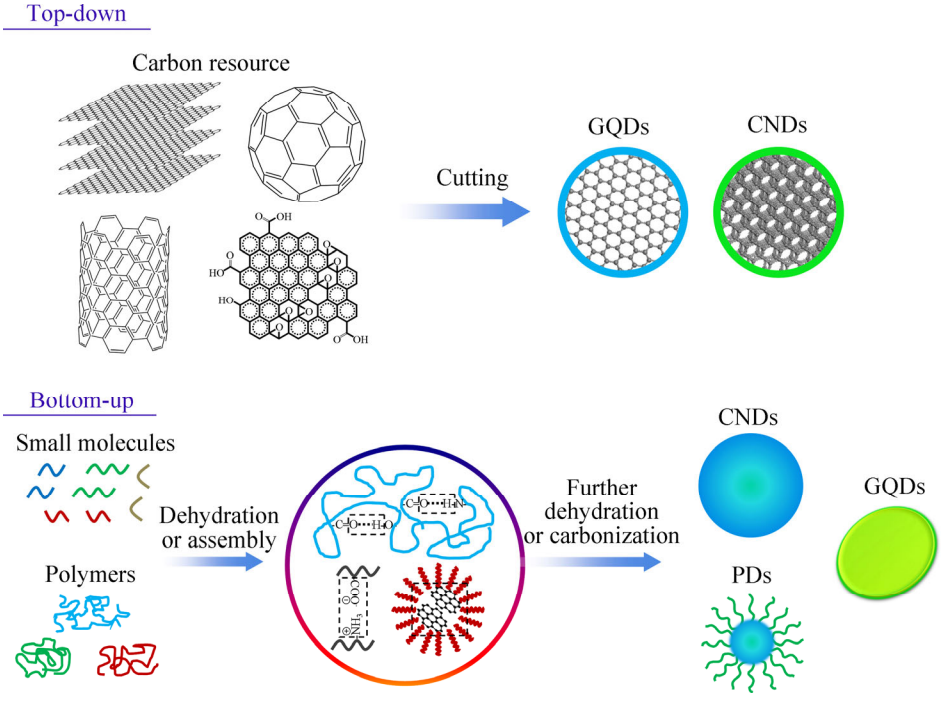

Figure 2 The main approaches to fabricating CDs: "Top-down" cutting from different carbon sources and "bottom-up" synthesis from organic molecules or polymers.

perchlorate (TBAP) [41], phosphate buffered saline (PBS)/water [42, 43], etc. The electric field peels off nanosized carbon from the electrode through graphite layer intercalation and/or a radical reaction.

In hydrothermal/solvothermal/special oxidation methods, some oxidized carbon resources such as GO and oxidized CNTs that possess defect-based chemical groups (oxygen-based groups) are cut into pieces at high temperature and pressure [30, 34]. Some special oxidation methods, such as a photo-Fenton reaction of GO to GQDs [44], can also break up GO. GQDs prepared by mask-assisted RIE in particular is an efficient approach for precisely controlling the size and surface chemistry of CDs [38], resulting in an ideal model system for clarifying the PL mechanism.

2.3 "Bottom-up" synthesis from organic molecules or polymers

The "bottom-up" methods are efficient routes to produce fluorescent CDs on a large scale (Fig. 2). For example, small molecules and polymers may undergo dehydration and further carbonization to form CNDs and PDs. The applied molecules always possess –OH, –COOH, –C=O, and $–NH_2$ groups, which can dehydrate at elevated temperatures. There are many approaches for carrying out the dehydration and carbonization processes, such as hydrothermal [45], microwave [46], and combustion [47] methods, pyrolysis in concentrated acid [48], carbonization in a microreactor [49], enhanced hydrothermal (microwave-hydrothermal [50] and plasma-hydrothermal [51]) methods, and so on. It is difficult to control these formation processes, resulting in CDs with polydispersity. However, using designed precursors may allow us to accurately obtain GQDs with the desired molecular weight and size, such as intramolecular oxidative polycyclic aromatic hydrocarbons (PAHs). Although organic-synthesized GQDs are the perfect model for understanding the PL mechanism of fluorescent carbon materials, the complicated synthesis method and variations in fluorescence as compared with common fluorescent CDs reduce their usefulness [52].

2.4 Surface functionality or passivation

Prepared CDs always possess many reactive groups, which can be modified by other chemical groups. Functionality and passivation can be used to enhance the quantum yields (QYs) of CDs, change the PL emission, and meet the requirements of special applications. The QYs of raw CDs used to be very low, making them difficult to use in applications; even detecting these CDs was difficult. Sun's group pioneered the use of NH_2–polyethylene glycol (PEG) passivation to elevate the PL QY of CNDs [53]. Zhu et al. used a similar method to enhance the PL properties of GQDs [54]. Yang's group used the cross-linked route to enhance the PL properties of PDs; bare polyethyleneimine (PEI) possessed little fluorescence, whereas cross-linked PDs had an elevated PL QY [55]. Surface or edge modification has also been used to tune the PL emission of CDs. For example, the green emission can be changed to a blue emission by surface reduction [56].

3 Chemical and physical properties

3.1 Chemical structure

As mentioned in the discussion of categories and synthesis routes, there are diversiform fluorescent CDs and various synthesis routes to obtain these materials. As a result, the chemical structures of CDs are diverse according to the different synthesis approaches. For example, GQDs possess single or a few graphene layers and connected chemical groups on the edges. They are anisotropic, with lateral dimensions larger than the height. Owing to the existence of a carbon core, GQDs possess certain crystallinity, with an average lattice parameter of 0.24 nm (Fig. 3(a)), which corresponds to (100) spacing of single graphene dots on lacey support films [35]. CNDs are always spherical, and they are divided into carbon nanoparticles without a crystal lattice and CQDs with an obvious crystal lattice [57]. The typical interlayer distance of CQDs is ca. 0.34 nm, which corresponds to (002) spacing of the crystalline graphite (Fig. 3(b)). PDs are an aggregation/assembly or cross-linked polymers from linear non-conjugated polymers. In addition, the carbon core and grafted polymer chains can also form PDs. All of the CDs possess connected or modified chemical groups on the surface, such as oxygen-based,

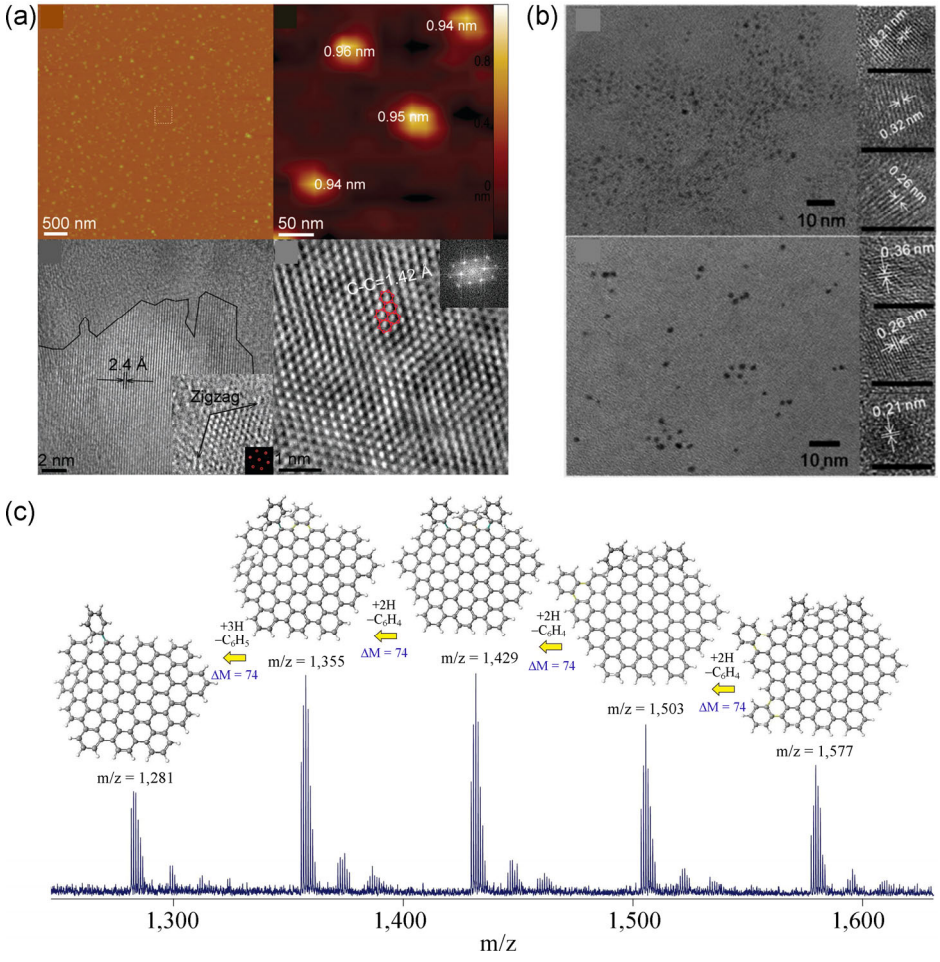

Figure 3 Selected typical structures of CDs. (a) Anisotropic GQDs with a single-layer carbon structure, with a height less than 1 nm and a lattice spacing of 0.24 nm. Reproduced by permission of Royal Society of Chemistry from Ref. [35]. (b) High-resolution TEM images of the CNDs. Reproduced by permission of American Chemical Society from Ref. [57]. (c) Possible stable structure for each molecular structure of the GQDs that corresponds to the observed MALDI-TOF mass pattern Reproduced by permission of Wiley-VCH from Ref. [58].

amino-based groups, polymer chains, etc. The direct characterization methods for the carbon core include high-resolution TEM (HRTEM), Raman spectroscopy, and X-ray diffraction (XRD). To evaluate the grafting of chemical groups, Fourier transform infrared (FTIR), X-ray photoelectron spectroscopy (XPS), nuclear magnetic resonance (NMR), matrix-assisted laser desorption ionization time-of-flight (MALDI-TOF) (Fig. 3(c)), and element analysis are used to determine the general structure [58]. As a result, these types of fluorescent CDs are not "pure" carbon materials. The hybridization and coefficient between the carbon core and surrounding chemical groups play a leading role in the PL behavior of these CDs.

3.2 Optical properties

Despite the diversity of the structures, CDs possess some similar optical properties in terms of their absorption and fluorescence. Herein, we will just summarize the common optical properties rather than consider specific examples. CDs typically show strong optical absorption in the UV region (230–320 nm), with a tail extending into the visible range. For the carbon core, a maximum peak at ca. 230 nm is ascribed to the π–π* transition of aromatic C–C bonds, whereas a shoulder at 300 nm is attributed to the n–π* transition of C=O bonds or other connected groups [59]. In addition, the connected chemical groups may

contribute to the absorption at the UV–visible regions. The observed deviations in absorption spectra data, at least to some extent, indicate differences in the compositions or structures of different hybridization derivatives.

The PL properties of CDs are the most important issue in terms of investigating the PL mechanism and adapting CDs for novel applications. Generally, the emission spectra of CDs are roughly symmetrical on the wavelength scale. The emission peaks of CDs are usually wide, with large Stokes shifts as compared with the emission of organic dyes. The emission peak position is always related to the excitation wavelength, which is known as wavelength-dependent behavior. This behavior may result from the wide distribution of differently sized dots and surface chemistry, different emissive traps (salvation effect), or a mechanism currently unresolved [60]. Fortunately, the excitation-dependent PL behaviors can be applied in multicolor imaging applications [61, 62].

The PL of CDs is a property similar to that of semiconductor quantum dots (QDs), but fluorescent nanoparticles possess many differences. First, it is inefficient to tune the PL color by controlling the size of CDs. In most situations, the PL color of CDs is relative to the surface groups rather than the size. The most common CDs have strong PL from blue to green, and a few CDs possess optimal emission in long-wavelength regions [23, 28, 63]. Another main difference between CDs and QDs is that the PL bandwidth of CDs is much wider. This wide peak may result from the inhomogeneous chemical structure and diverse PL centers.

QY is the number of emitted photons relative to the number of absorbed photons. CDs possessed rather low QYs (even lower than 1%) when they were first discovered. After surface modification or passivation, the QY can be dramatically increased. The enhanced PL properties are attributed to the strongly PL centers on the surface, the synergy between the carbon core and the chemical groups, or solely to the presence of fluorophores [64]. The QYs of CDs have continually improved year by year. Generally, QY depends on the synthesis route and the surface chemistry.

Most CDs possess good photostability, which is the result of the carbon core-based PL center. Neither blinking nor meaningful reductions in PL intensity are observed in such CDs after continuous exposure to excitation (Fig. 4(a)) [37]. However, for CDs with molecule-state emission, the PL intensity decreases dramatically after high-power UV exposure [65]. Some special luminescence behaviors of CDs can be observed in some situations, such as with electrochemical luminescence (ECL, Fig. 4(b)) [33]. The ECL mechanism of CDs is suggested to involve the formation of excited-state CDs via electron-transfer annihilation of negatively charged and positively charged CDs. Although up-conversion PL (two-photon absorption and anti-Stokes PL) has been reported [23, 54], it is quite important to establish a proper characterization system in order to investigate these types of properties because some so-called "up-conversion PL" in CDs could be due to the excitation of second-order diffraction light (wavelength $\lambda/2$) from the monochromators in the fluorescence spectrophotometer [66, 67]. Amplified spontaneous green emission and lasing emission has also been observed from CNDs (Fig. 4(c)) [68], and the high PL quantum yield and small overlap between the absorption and emission of CDs in an ethanol solution were the key factors in achieving lasing emission. These special optical properties may lead to novel application of different types of CDs.

In addition to direct characterization, there are several indirect approaches for studying PL mechanisms in CDs. pH-Dependent and solvent-dependent PL is very important for investigating the emission behaviors of CDs (Figs. 4(d)–4(e)) [30, 34]. The molecule state is affected under both strongly acidic and strongly basic atmospheres, whereas the PL intensity of the carbon core–edge state may increase owing to protonation or deprotonation of the functional groups. The PL quench behaviors of CDs are another important tool for understanding the PL mechanism (Fig. 4(f)) [69].

3.3 Biological toxicity

The toxicity of CDs is of extraordinary concern because of their potential for use in bio-based applications [12, 19, 70, 71]. Bio-imaging-based applications *in vitro*/*in vivo* must be non-toxic and biocompatible [72]. Over the last several years, metal-based QD bio-imaging methodologies have appeared, together with toxicity concerns because of the use of intrinsically toxic

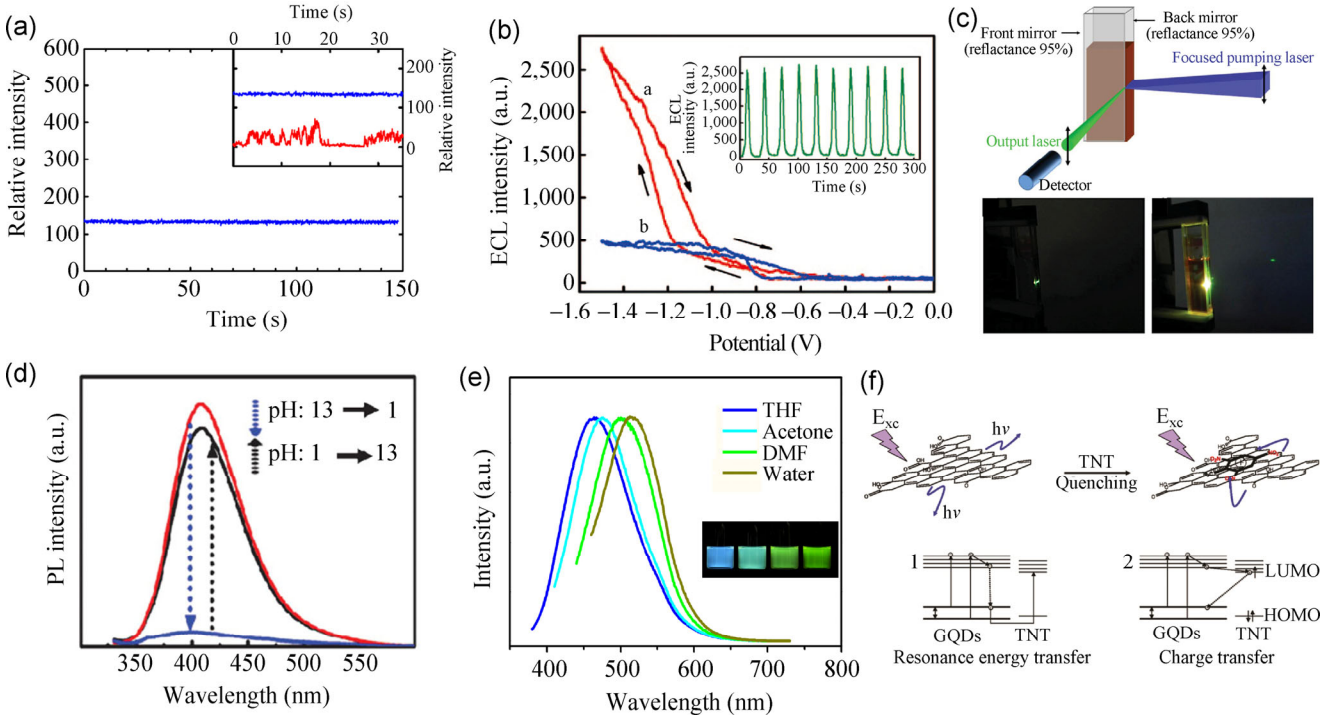

Figure 4 Selected optical properties of CDs. (a) The photo-stability of CNDs. Reproduced by permission of American Chemical Society from Ref. [37]. (b) ECL of CNDs in aqueous 0.1 M PBS solution in the presence and absence of 1 mM $K_2S_2O_8$. Inset: ECL responses of CNCs/$S_2O_8^{2-}$ obtained during a continuous potential scan at 0.1 V·s^{-1}. Reproduced by permission of American Chemical Society from Ref. [33]. (c) Schematic diagram of experimental setup for optical pumping investigations of the CND-based laser device. The images below show the operating CND-based laser device under 355 nm laser pumping at 30 kW·cm^{-2} and 90 kW·cm^{-2}. Reproduced by permission of Wiley-VCH from Ref. [68]. (d) The pH-dependent behavior of GQDs. Reproduced by permission of Wiley-VCH from Ref. [34]. (e) The PL solvent-dependent behavior of GQDs. Reproduced by permission of Royal Society of Chemistry from Ref. [30]. (f) Schematic of a Förster Resonance Energy Transfer (FRET)-based GQD sensor for detection of TNT: quenching mechanism through (1) resonance energy transfer from the GQD donor to the TNT acceptor and (2) charge transfer from the excited GQDs to TNT. Reproduced by permission of Elsevier from Ref. [69].

elements such as cadmium. As compared with metal-based QDs, GQDs are composed of an intrinsically non-toxic element, carbon, which makes them a particularly useful and promising bio-analytical tool. Toxicity studies have been conducted by various research groups, and CDs appear to have low toxicity *in vitro* and *in vivo*. So far, the inherent toxicities of CDs have been evaluated by the cell-viability assay. The results indicate that GQDs, CNDs, and PDs possess excellent biocompatibility and low cytotoxicity [15, 29, 30, 53, 73–75]. Carboxylated GQDs did not cause apparent toxicities in rats at different dosages (5 and 10 mg·kg^{-1}) over 22 days, as evidenced by blood biochemistry and hematological analysis [76]. No severe symptoms of inflammation were observed in the liver, kidney, spleen, heart, or lungs 22 days after the administration of the carboxylated GQD nano-particles. All the evidence points to the great potential of CDs for *in vitro* and *in vivo* imaging studies.

4 PL mechanism of GQDs

GQDs are the simplest CDs, with a single-layer carbon core with connected chemical groups on the surface or edges. As a result, GQDs are the ideal model to investigate the PL mechanism of CDs. To explain the PL mechanism of GQDs, the PL behavior of chemically derived GO is introduced first because GO is an important raw material for GQD preparation and thus GO and GQDs possess similar chemical structures. GO contains oxygen-based functional groups, either on the basal plane or at the edges. Therefore, the 2–3 nm aromatic sp^2 domains are surrounded by a linearly aligned epoxy and hydroxyl-boned sp^3 C–O

matrix [5, 77]. Because GO has such a structure, the fluorescent properties are determined by the π states of the sp^2 sites. The π and π* electronic levels of the sp^2 clusters, which are influenced by the band gap of the σ and σ* states of the sp^3 matrix, are strongly confined. Radiative recombination of electron–hole (e–h) pairs in such sp^2 clusters can facilitate fluorescence [78]. Because of the existence of a wide size distribution of sp^2 domains in GO, the band gaps of different sizes of sp^2 cover a wide range, leading to a wide PL emission spectrum from visible to near infrared (Fig. 5). Many groups have investigated the fluorescence of GO and reduced GO (r-GO). For example, Luo et al. proposed that bond distortions may contribute to the fluorescence of GO and r-GO [79]. Gokus et al. observed visible luminescence in oxygen plasma-treated graphene and attributed the emission to CO-related localized electronic states at the oxidation sites [4]. Furthermore, Galande et al. studied the pH-dependent fluorescence of GO, and they suggested the emission of quasi-molecular fluorophores in such types of materials [80]. They found that the excited state of the fluorophore species was protonated in acidic media, which makes the PL spectra different in acidic and basic solutions. This kind of quasi-molecular fluorophore is caused by carboxylic acid groups that are electronically coupled with the surrounding graphene core sheets [81].

Similar to GO, GQDs possess more defects, oxygen groups, and functional groups on the surface. The fluorescence results obtained for GO can be used to understand these emissions in GQDs. Excitons in graphene have an infinite Bohr diameter. Thus, graphene fragments of any size will show quantum confinement effects. As a result, GQDs have a non-zero band gap and PL on excitation. This band gap is tunable by modifying the size and surface chemistry of the GQDs [6]. Considerable development in the preparation of GQDs has been witnessed in the last five years, and researchers have discovered reasonable PL mechanisms: the surface/edge state and conjugated π-domains.

4.1 Surface/edge state in GQDs

The surface/edge state contains triple carbene at the zigzag edges, oxygen-based groups on the graphene core, and resonance of amine moieties and the graphene core.

When graphene sheets are cut along different crystallographic directions, diverse types of edges (armchair and zigzag edges) can be obtained. The edge type plays an important role in determining the electronic, magnetic, and optical properties of the GQD. Ritter et al. stated that predominantly zigzag-edge GQDs with average dimensions of 7–8 nm are metallic owing to the presence of zigzag-edge states and that

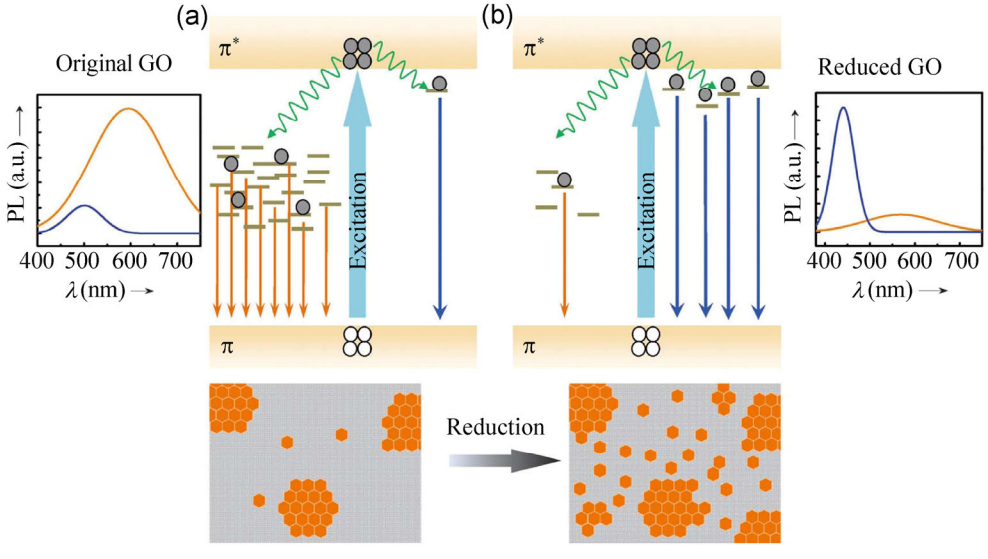

Figure 5 Proposed PL emission mechanisms of (a) the predominant "red emission" in GO from disorder-induced localized states and (b) the predominant "blue emission" in reduced GO from confined cluster states. Reproduced with permission of Wiley-VCH from Ref. [78].

Graphene nanoribbons (GNRs) with a higher fraction of zigzag edges exhibit a smaller energy gap than those with a predominantly armchair-edge ribbon of similar width [82]. Radovic and Bockrath reported that the zigzag sites are carbene-like, with a triplet ground state being the most common, whereas the armchair sites are carbyne-like, with a singlet ground state being the most common [83]. Pan et al. suggested that the blue PL exhibited by hydrothermally cut GQDs might be attributed to free zigzag sites, with a carbine-like triplet ground state described as $\sigma^1\pi^1$ [34]. Under acidic conditions, the free zigzag sites of the GQDs are protonated, forming a reversible complex between the zigzag site and H^+ and leading to the breaking of the emissive triple carbene state and PL quenching (Fig. 4(b)). On the other hand, the PL recovers because the free zigzag sites are restored under alkaline conditions. Lin et al. prepared GQDs with a size of approximately 20 nm by exfoliating and disintegrating CNTs or graphite flakes [35]. The obvious single layer and clear zigzag edge were confirmed using AFM and bright-field high-resolution TEM. A newly opened band gap arose from the triple carbenes at the zigzag edges, corresponding to the transition from the highest occupied molecular orbital (HOMO) to σ and to the π orbital of the lowest unoccupied molecular orbital (LUMO) in the triple carbenes. These two types of GQDs with sizes of 9.6 nm and 20 nm, respectively, possessed similar absorption and emission behavior, which proved that the PL mechanism was determined by the triple carbene at the zigzag edges instead of by the quantum confinement effects (Fig. 6(a)).

Pan et al. also used single-particle spectroscopic measurements to investigate the PL behaviors of GQDs [84]. As schematically shown in Fig. 6(b), photo-excited electrons through the π–π* transitions were

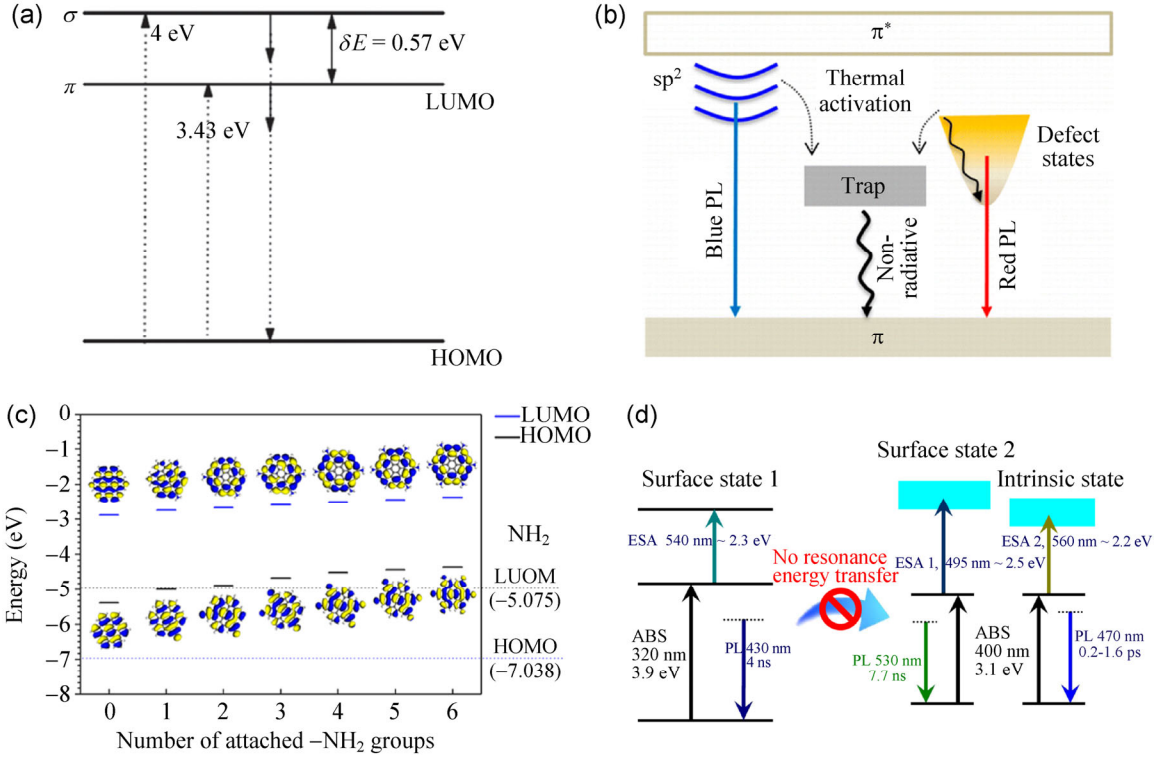

Figure 6 Surface/edge states in GQDs. (a) Free zigzag emission mechanism of the GQDs. Reproduced with permission of Royal Society of Chemistry from Ref. [35]. (b) Energy level structures to explain the optical behaviors of photoexcited electrons in GQDs, including their radiative recombination from discrete sp^2-related states and continuous defect states, thermally activated decay into non-radiative traps, and non-radiative relaxation from higher- to lower-lying defect states. Reproduced with permission of American Chemical Society from Ref. [84]. (c) HOMO and LUMO energy levels of GQD–$(NH_2)n$. Black and blue lines indicate HOMO and LUMO levels, respectively. The dotted lines denote the HOMO and LUMO energy level of NH_2. Reproduced with permission of American Chemical Society from Ref. [85]. (d) The PL picture in green-fluorescence GQDs. (ABS: absorption; ESA: excited-state absorption). Reproduced with permission of Wiley-VCH from Ref. [89].

proposed to relax into either the sp^2 energy levels or the defect states (what we call the surface state), giving rise to blue or long-wavelength PL, respectively. The blue emission might bear discrete features owing to the quantum confinement effect (QCE) of electrons inside the sp^2 carbon domains. The long-wavelength emission is related to the the hybrid structure comprising the oxygen functional groups (at the edges and/or on the basal planes) and the graphene core. Despite noticeable differences in the size and the number of layers from particle to particle, all of the GQDs studied possessed almost the same spectral line shapes and peak positions. This suggests that the PL of these GQDs was caused by their surface state.

In addition to oxygen-based groups, amine-based groups also contribute to the surface state in GQDs. In the work of Tetsuka et al., the ammonia-assisted hydrothermal method was used to prepare GQDs. The product was edge-terminated by a primary amine, allowing the electronic structure to be modified by the effective orbital resonance of the amine moieties and the graphene core [58]. For GQDs of the same size, the emission wavelength increased with increasing numbers of amine groups. Furthermore, the GQDs possessed high QYs because of the reduction of carboxylic and epoxide groups, which act as non-radiative electron–hole recombination centers. Combining the experimental results and *ab initio* calculations, the primary amines at the edges of GQDs were shown to have a higher HOMO than hydrogen-terminated groups owing to the strong orbital interaction with the $–NH_2$ groups. The resonance feature between the delocalized π orbital and the molecule orbital in the $–NH_2$ groups results in a narrowing of the optical band gap. Such amino-containing GQDs have also been reported by other groups. Jin et al. reported that functionalized GQDs exhibited a redshift in the PL emission spectrum as compared to non-functionalized GQDs (the PL emissions of the amine-functionalized GQDs also shifted with changes of the pH owing to the protonation and deprotonation of the functional groups) [85]. Calculations from density functional theory (DFT) illustrated that PL shifts resulted from charge transfers between the functional groups and GQDs, which can tune the band gap of the GQDs. The band gap of the GQDs decreased to 2.254 eV when they were functionalized by one amino group. Also, the band gap gradually decreased with the increasing number of $–NH_2$ groups (Fig. 6(c)). Kumar et al. also investigated the PL behaviors of amino-functionalized GQDs. First-principles calculations suggested that primary amine-edge termination (NH_2) resulted in formation of an additional interband ca. 3.28 eV within the energy gap owing to p-orbital hybridization of C–N atoms at the edge sites [86]. Feng and co-workers proved that 1,2-ethylenediamine functionalization on the surface of GQDs can form a specific cyclic structure that facilitates proton transfer from the ammonium moiety to the conjugated structure, thus leading to the largest enhancement of fluorescence in the serial of samples [87].

The mechanism of GQD emission was further investigated with femtosecond transient absorption spectroscopy and femtosecond time-resolved fluorescence dynamics measured by a fluorescence upconversion technique and a nanosecond time-correlated single-photon counting technique by Wang's and Yang's groups [88, 89]. They found that two independent molecule-like states and a dark intrinsic state existed in solvothermally synthesized GQDs, as shown in Fig. 6(d). The intrinsic state is attributed to the graphene core and its PL occurs at approximately 470 nm, with a dominant short lifetime and low PL QY. Two additional irrelevant molecule-like states at approximately 320 nm and 400 nm exhibited blue fluorescence, with a peak at ca. 430 nm, and green fluorescence, with a peak at ca. 530 nm. The three types of emission states constitute the fascinating PL of green-fluorescence GQDs. In related work, Yang's group found that the PL of GQDs could be changed from green emission to blue emission by tuning the surface chemistry [90]. Through modification of the GQDs, the connected alkylamines transferred the –COOH and epoxy of GQDs into –CONHR and –CNHR, both of which can reduce the non-radiative recombination induced by the –COOH and epoxy groups [91] and transfer GQDs from defect-state emission into intrinsic-state emission. In the reduction method, the carbonyl, epoxy, and amino moieties were changed into –OH groups, which suppressed the non-radiative process and further enhanced the integrity of the π-conjugated system (it also reduced the defects). As a result, intrinsic-state emission (containing both the intrinsic and blue molecule-like

state observed in transient absorption, TA) rather than defect-state emission plays a leading role. Blue and green emissions of GQDs and graphene oxide quantum dots (GOQDs) were also reported by Seo et al. [92]. They revealed that the green luminescence of GOQDs originates from defect states with oxygenous functional groups, whereas the blue luminescence of GQDs is dominated by intrinsic states in the highly crystalline structure.

The surface/edge state of PL in the GQDs has also been investigated by other groups [93–98]. For example, Lingam et al. found evidence for edge-state PL in solvothermally synthesized GQDs. If the edge of the GQDs was destroyed or disappeared, the PL intensity decreased to the point that it vanished [99]. All similar work proved that the surface state (or edge state) was the key PL mechanism in these types of GQDs. In addition, for some types of GQDs, the functional surface state could be considered as special polyaromatic fluorophores.

4.2 Quantum confinement effect of conjugated π-domains in GQDs

In the last section, the surface state rather than the intrinsic graphene core state was shown to play a leading role in the PL behavior of related GQDs. However, for GQDs with a perfect graphene core and fewer surface chemical groups, the band gap of conjugated π-domains is thought to be the true intrinsic PL center. A major feature of QDs is the QCE, which occurs when quantum dots are smaller than their exciton Bohr radius [100]. DFT calculations have shown that the band gap increases to approximately 2 eV in GQDs consisting of 20 aromatic rings and 7 eV for benzene (Fig. 7(a)) [5]. In other words, the PL emission of the GQDs can be tuned by adjusting the size of the conjugated π-domains. Typically, because the particles are smaller, the luminescence energies are blue-shifted to a higher energy.

First, GQDs prepared by the organic solution method

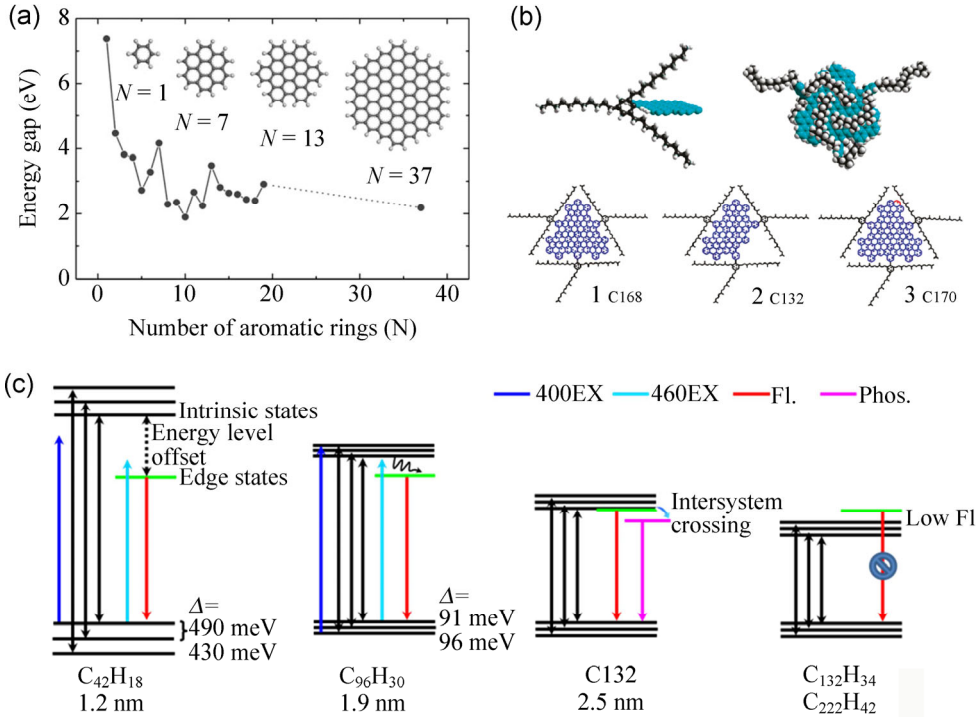

Figure 7 Quantum confinement effect of conjugated π-domains in GQDs. (a) Energy gap of π–π* transitions calculated based on DFT as a function of the number of fused aromatic rings (N). The inset shows the structures of the graphene molecules used for the calculation. Reproduced with permission of Wiley-VCH from Ref. [5]. (b) Solubilization strategy for colloidal GQDs. Reproduced with permission of American Chemical Society from Ref. [101]. (c) The suggested energy levels of $C_{42}H_{18}$, $C_{96}H_{30}$, C_{132}, $C_{132}H_{34}$, and $C_{222}H_{42}$. The size-dependent energy levels in these H-passivated small GQDs are in agreement with the molecule orbital calculation. The intrinsic state depends on size. The energy-level offset between the intrinsic state and the edge state determines its optical properties. The energy level of C_{132} was determined from the reported paper [21]. Reproduced by permission of Elsevier from Ref. [104].

are introduced because they possess special electronic and optical properties, making them suitable models for investigating the PL of GQDs exhibiting the QCE. Recently, Li et al. reported the synthesis and optical characterization of colloidal GQDs with a uniform and tunable size through organic chemistry routes [21]. The prepared GQDs consisted of graphene moieties containing 168, 132, and 170 conjugated carbon atoms (Fig. 7(b)) [101]. The synthesis was based on oxidative condensation reactions developed by Scholl, Müllen, etc. [102]. GQDs consist of light atoms, and thus they have a small dielectric constant and weak spin-orbit coupling. These characteristics lead to strong carrier–carrier interactions and electronic states with well-defined spin multiplicity. As a result, GQDs have a much larger energy band than other inorganic semiconductor QDs of similar size. This is why most GQDs possess PL in the range from blue to green. Furthermore, the size-dependent, discrete excitonic levels could significantly slow the relaxation of highly excited states in GQDs owing to a phonon bottleneck. In addition, strong carrier–carrier interactions could lead to the generation of more than one exciton with one photon absorbed, a process particularly useful for improving the efficiency of photon-generated carriers [103]. The singlet–triplet splitting of GQDs was determined to be ca. 175 meV, and intersystem crossing was so efficient that it competed with internal conversion among states with the same multiplicity. As a result, the GQDs emitted both fluorescence and phosphorescence [101]. Since triplet states have a significantly longer lifetime, they could profoundly affect the chemical reactivity and processes such as charge transfer or exciton migration in the GQD-based system. Yang et al. investigated the photophysics of organically synthesized GQDs ($C_{42}H_{18}$, $C_{96}H_{30}$, $C_{132}H_{34}$, and $C_{222}H_{42}$), and they found that the intrinsic state depended on size, whereas the energy-level offset between the intrinsic state and the edge state determined the optical properties of the GQDs (Fig. 7(c)) [104]. As a result, the green fluorescence of $C_{42}H_{18}$ and $C_{96}H_{30}$ not only depended on the size, it also resulted from the bright edge state. If the energy-level offset between the intrinsic state and the edge state is large enough, the fluorescence is dominant. If the energy-level offset is small enough (meeting the thermal activation condition, ca. k_BT), the long carrier lifetime in the intrinsic state could facilitate intersystem crossing from a singlet-excited edge state to a triplet-excited edge state, such as for the abovementioned C_{132}. In the cases of $C_{132}H_{34}$ and $C_{222}H_{42}$, the intrinsic state possibly decreased and was lower than the edge state; as a result, the GQDs lost the expected fluorescence.

The size-dependent PL of GQDs prepared by "nano-methods," in which the PL is not controlled by the QCE, is now introduced. Peng et al. prepared three kinds of GQDs with sizes of 1–4 nm, 4–8 nm, and 7–11 nm by varying the reaction temperatures. These GQDs emitted PL ranging from blue and green to yellow, as shown in Figs. 8(a)–8(b) [24]. GQDs prepared via acidic oxidation from carbon black showed PL transitions from green to yellow as their sizes increased from 15 to 18 nm. Kim et al. presented size-dependent shape/edge-state variations of GQDs and visible PL showing anomalous size dependences (Fig. 8(c)) [105]. Upon varying the average size of the GQDs from 5 to 35 nm, the peak energy of the absorption spectra monotonically decreased (Fig. 8(d)). The peak energy and shape of the PL spectra are strongly dependent on the size of the GQDs. All PL spectra show similar size-dependent peak shifts, almost irrespective of excitation wavelength except 470 nm. The PL peak energy decreases as the QD diameter increases up to ca. 17 nm, which is consistent with the QCE. However, when the diameter is larger than ca. 17 nm, the PL peak energy increases with increasing diameter; in other words, the QCE no longer holds. These results originate from changes to the edges. For diameters <17 nm, the majority of GQDs have a circular/elliptical shape, with mixed zigzag and armchair edges; however, for diameters >17 nm, the edges exhibit a polygonal shape with mostly armchair edges. These changed edges disturb the evolution between the QCE and the size of the GQDs. As mentioned above, the greater number of armchair edges as compared with zigzag edges could result in larger energy gaps for graphene materials [82].

Most of the reported GQDs possessed diameters greater than 5 nm and strongly visible PL emission. However, based on DFT results, the band gap energies of GQDs with diameters greater than 5 nm are no higher than 1.0 eV [106]. The visible PL found in

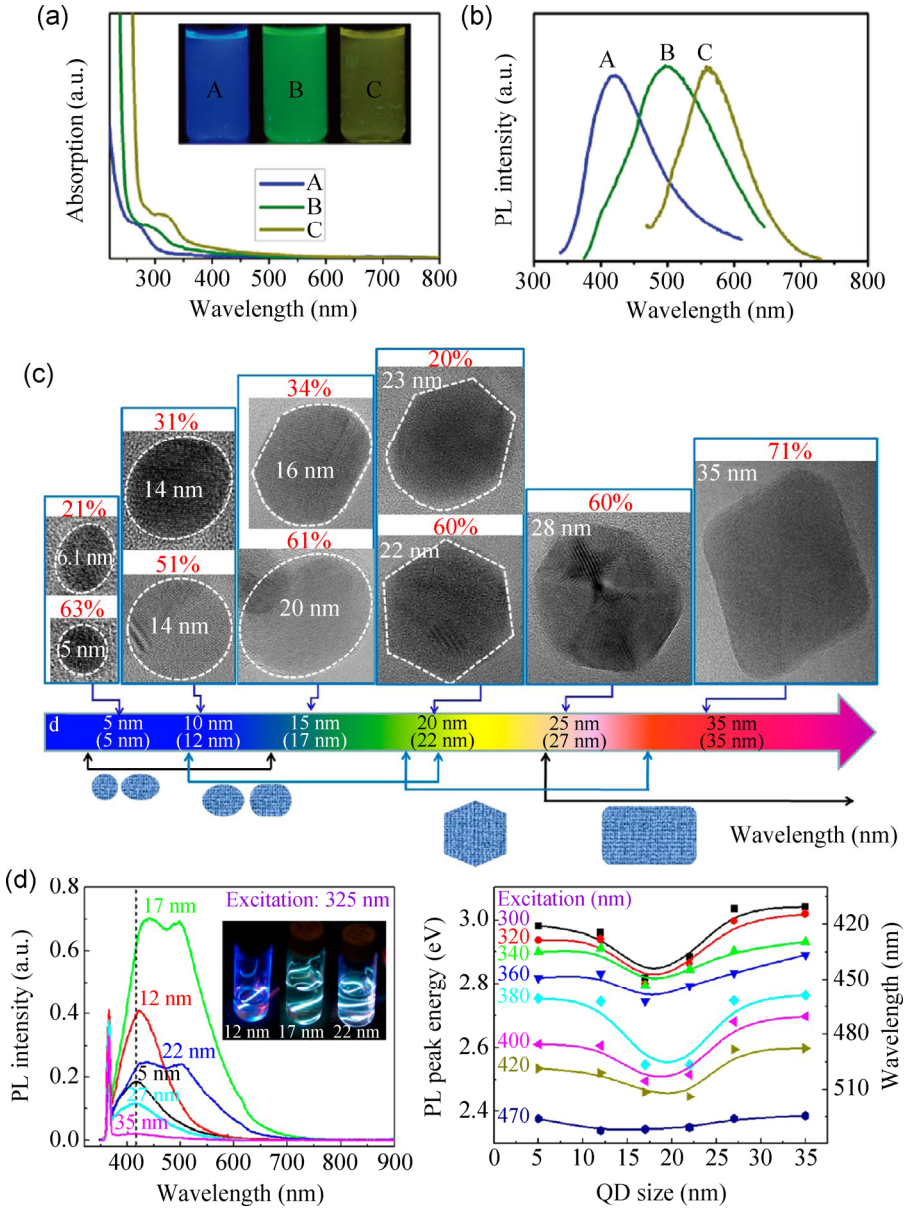

Figure 8 (a) UV-vis spectra of GQDs A, B, and C, which correspond to synthesized reaction temperatures at 120, 100, and 80 ˚C, respectively. Inset is a photograph of the corresponding GQDs under UV light with 365 nm excitation. (b) PL spectra of GQDs with different emission colors excited at 318, 331, and 429 nm. Reproduced with permission of American Chemical Society from Ref. [24]. (c) HRTEM images of GQDs for their major shapes and corresponding populations (p) with increasing average size of GQDs. Here, the dotted line indicates a GQD region and p is defined as the ratio of the number of GQDs with a major shape at each average size. (d) Size-dependent PL spectra excited at 325 nm for GQDs with average sizes of 5–35 nm in deionized (DI) water. Also shown is the dependence of PL peak shifts on the excitation wavelength from 300 to 470 nm for GQDs with average sizes of 5–35 nm. Reproduced with permission of American Chemical Society from Ref. [105].

GQDs could be explained by the minimization of thermalization owing to electron–phonon scattering or by formation of an excited-state relaxation channel, resulting in inelastic light scattering by electric doping [100, 107]. By size-dependent shape/edge-state variations of GQDs, the electronic transitions can be modified in nanometer-sized GQDs to produce strong visible PL emissions in a controlled fashion. The high-energy PL of GQDs is especially efficient owing to the unique properties of graphene: fast carrier–carrier

scattering dominates over electron–phonon scattering. This facilitates direct recombination of excited e–h pairs, producing high-energy PL before thermalization of the carriers with the lattice [108]. The high Coulomb scattering rate of graphene, which is attributed to the strongly reduced dielectric screening in the two-dimensional structure, is also essential for producing high-density non-equilibrium carriers responsible for the strong e–h recombination.

Moreover, because the surface/edge state-derived PL emissions are relatively brighter, there may be a general risk for their contaminating the observed band gap fluorescence in GQDs [86]. As a result, much of the experimentally observed PL of GQDs was surface/edge-state PL. For clear investigation on the QCE of GQDs, organic synthesis and nanolithography-based routes for fabricating perfect sample will be highly desired in the near future.

Chromatographic separation is also a powerful tool for investigating the PL mechanism of GQDs. For example, Zhu et al. pioneered the use of column chromatography to separate GQDs with a tuned oxidation degree; as a result, the separated GQDs possessed PL from blue to green [31]. Matsuda and co-workers developed size-exclusion high-performance liquid chromatography (HPLC) to separate the prepared GQDs [109]. Drastic changes in the PL spectra of GQDs from UV to red are observed according to the difference in their overall sizes. Discrete changes in emission wavelength indicate that the PL change comes from differences in the number of small sp^2 fragments of various sizes or from shapes embedded in the GQDs.

It is also highly important to clarify the PL mechanism of GQDs by theoretical calculations. For example, Alam Sk et al. systematically investigated the PL properties of GQDs using DFT and time-dependent density functional theory (TDDFT) calculations [106]. The results revealed that the emission of zigzag-edged GQDs can cover the entire visible light spectrum by varying the diameter from 0.89 to 1.80 nm. Armchair edges and pyrrolic N-doping induce a blue-shift, whereas chemical functionalities and defects can cause a red-shifted PL. Furthermore, the isolated inhomogeneous sp^2 domains can widen the PL peaks of GQDs.

5 PL mechanism of CNDs

5.1 Quantum size effect in carbon quantum dots

There are a few studies concerned with the quantum size effect in CNDs. We would rather call these types of CNDs "CQDs." Kang et al. developed a current density-controlled electrochemical method to prepare CQDs. After further separation, CQDs 1.2–3.8 nm in size were obtained [23]. The PL properties varied sensitively with CQD size (Fig. 9(a)), with small CQDs (1.2 nm, center) giving UV light emission, medium-sized CQDs (1.5–3 nm) giving visible light emission (400–700 nm), and large CQDs (3.8 nm, center) giving near-infrared emission (Figs. 9(b)–9(j)). To further confirm these results and explain why these strong emissions came from the quantum-sized graphite fragments of CQDs, Kang et al. performed theoretical calculations to investigate the relationship between PL and cluster size. Figure 9k shows the dependence of HOMO–LUMO gaps on the size of the graphene fragments. As the size of the fragment increases, the gap gradually decreases. The gap energy in the visible spectral range was obtained from graphene fragments with diameters of 1.4–2.2 nm, which agrees well with the visible emission of CDs with diameters of <3 nm. Thus, they deduced that the strong emission of CDs comes from the quantum-sized graphite structure.

Lau and co-workers developed a novel method of preparing water-soluble monodispersed crystalline CQDs (which they called GQDs in their work) with diameters ranging from 1.5 to 3.9 nm ± 0.55 nm [110]. They proved that the larger the diameter of the GQD, the shorter the average lifetime. Rhee and Kwon developed size-controlled synthesis of CNDs using a "water-in-oil" emulsion as a self-assembled soft template [111, 112]. The micelles were micro-emulsions of water encapsulated by surfactant molecules in the immiscible oil; the size of the micelles could be regulated by the water–surfactant molar ratio. Thus, this reaction can offer size tunability and a narrow size distribution. They found that different-sized CNDs had different band gaps and hence exhibited diverse PL behaviors. The PL peak position was blue-shifted by approximately 25 nm upon increasing the size of the CNDs from 1.5 to 3.5 nm. These results, which are

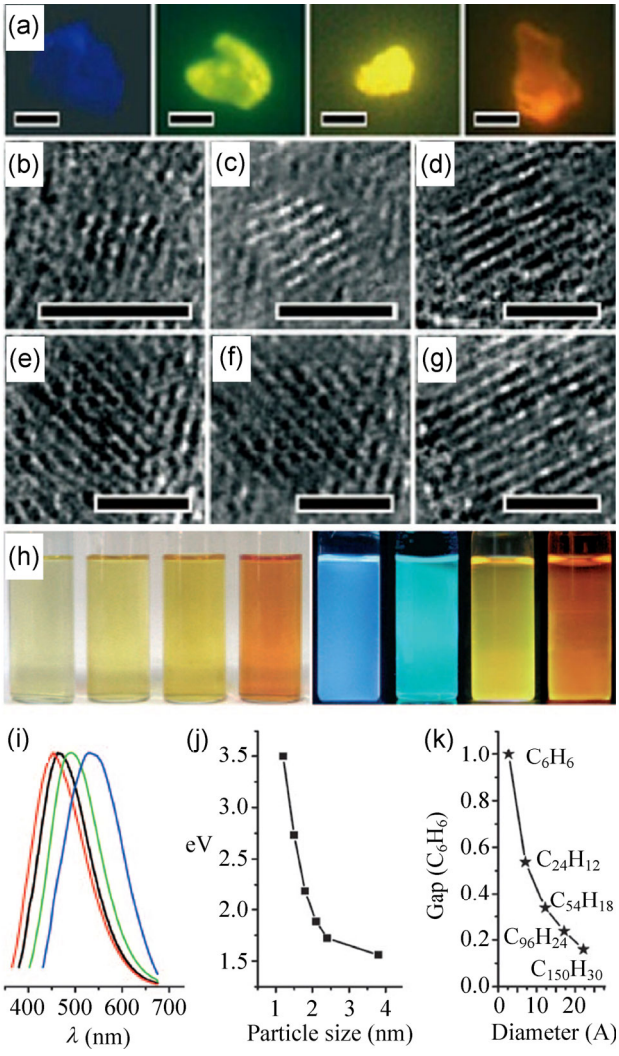

Figure 9 Quantum size effect in carbon quantum dots (CQDs). a) Fluorescent microscopy images of CQDs with an excitation wavelength of 360 nm (scale bar: 50 mm). (b)–(g) HRTEM images of typical CQDs with different diameters (scale bar: 2 nm). (h) Optical images of typical-size CQDs illuminated under white (daylight lamp) and UV light (365 nm). (i) PL spectra of typical-size CQDs: the red, black, green, and blue lines are the PL spectra for blue-, green-, yellow-, and red-emission CQDs, respectively. (j) Relationship between the CQD size and the PL properties. (k) HOMO–LUMO gap dependence on the size of the graphene fragments. Reproduced with permission of Wiley-VCH from Ref. [23].

opposite those of the quantum size effect, are further explained by the presence of sp^2 clusters with certain energy gaps and oleylamine ligands, which act as auxochromes to reduce the energy gaps. As a result, large CNDs with relative small ratios of ligand/sp^2 clusters possess larger band gaps as compared with small CNDs.

5.2 Surface state in CNDs

Functional groups have various energy levels, which may result in a series of emissive traps. When the light of a certain excitation wavelength illuminates the CNDs, a surface state emissive trap will dominate the emission. A higher degree of surface oxidation or other effective modification can result in more surface defects, resulting in a red-shifted emission. The surface state does not consist of isolated chemical groups but rather the hybridization of the carbon backbone and connected chemical groups. From the first report of CNDs [25], which were prepared via electrophoretic analysis and purification of fluorescent CNT fragments in 2004 (the CNDs were an oxidation-cut product with oxygen-based chemical groups on the surfaces), most PL centers of the reported CNDs were proven to be surface states. Sun and co-workers systematically investigated the surface passivation of CNDs by amino-polyethylene glycol (PEG). The CDs were initially produced via laser ablation of a carbon target in the presence of water vapor with argon as the carrier gas [37]. The authors proved that many organic molecules could provide surface passivation, which further proved that surface energy traps controlled the PL mechanism. Although the excitation may induce the band-gap absorption band, the resulting fluorescence was also controlled by the surface state emission (Fig. 10(a)) [113].

From then on, many oxidation-based surface states were directly attached during the process of preparing CNDs. In another words, oxygen-based groups on the carbon core were the primary surface state of CNDs. Mao and co-workers obtained colorful CNDs derived from oxidizing candle soot and further separation (top-down route). The PL, which ranged from violet to red, may have been induced by different surface oxidation [28]. CNDs with surface-state emission were also achieved by the bottom-up carbonization method, and the PL could be tuned from blue to green using different reaction conditions. It is very interesting that most surface-state emission studies focused on the blue–green range. Pang and co-workers proved that the surface states were the key factor in tuning the luminescence of electrochemical CNDs [41]. Red-shifted emissions were observed for CNDs with a high

surface oxidation degree. Zheng and other researchers also proved that the emission of CNDs can be changed from green to blue by surface reduction [56]. Furthermore, Richards and co-workers used single-particle fluorescence technology to investigate the PL fluctuations of oxidized/reduced CNDs [114]. They suggested that single dots can possess multiple fluorophore units associated with the CND core and oxygenated defect-related emissive traps. The majority of the reduced CND particles showed multiple levels of excited state, whereas the oxidized particles predominantly showed a single level. A possible explanation for this is that after the initial excitation, the energy is transferred from the higher energy absorbing site to a lower energy emissive site in the oxidized CND particles. In contrast, when CNDs are reduced, the low-energy emissive traps are entirely or partially removed, blocking energy-transfer pathways. In addition, the authors proved that the CNDs possessed photo-bleaching at the single- particle level, which is in contrast to the reported steady-state fluorescence characterization (Fig. 10(b)).

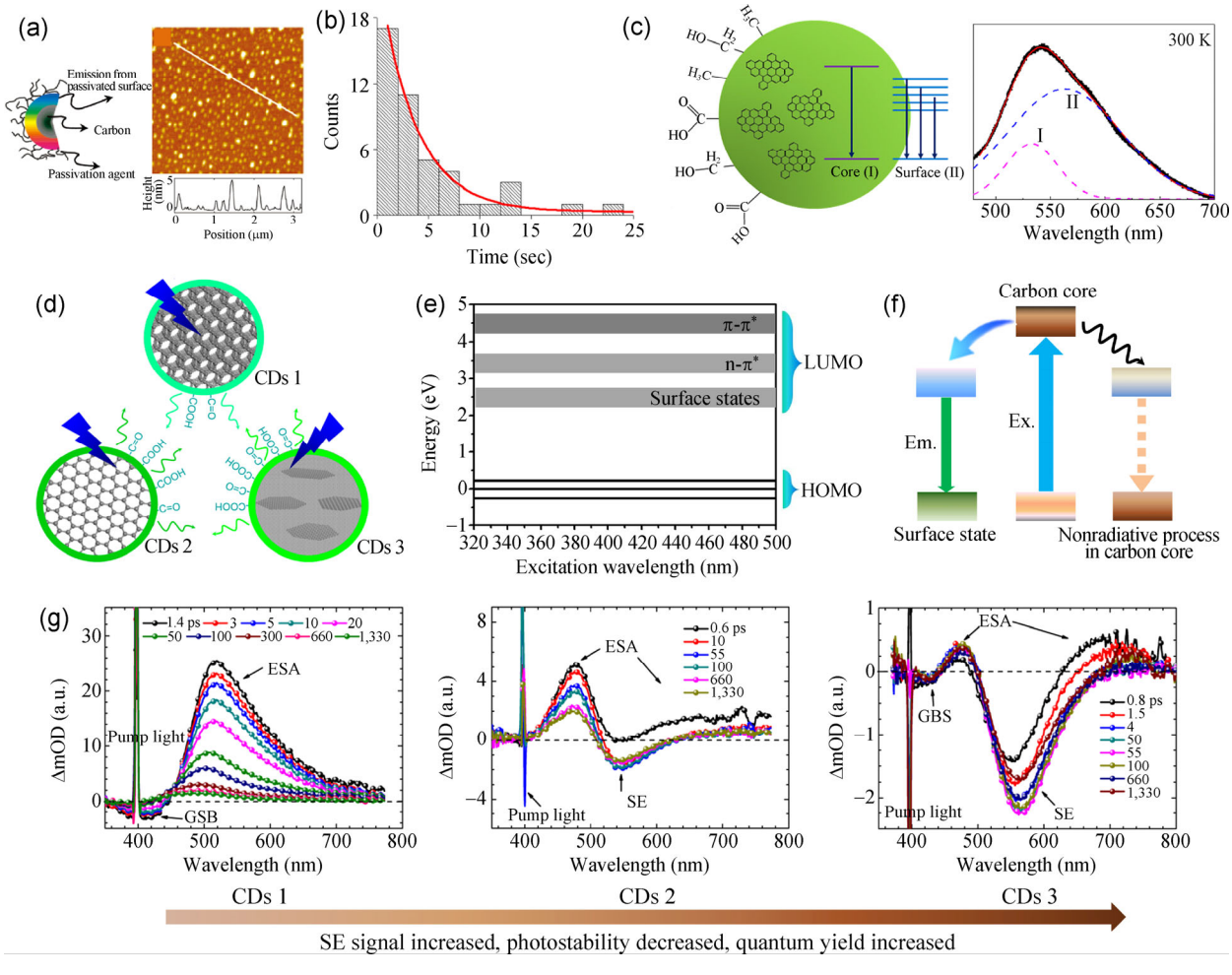

Figure 10 Surface state and carbon-core state in CNDs. (a) The CND structure and AFM topography image of CNDs on mica substrate with the height profile along the line in the image. Reproduced with permission of American Chemical Society from Ref. [53]. (b) Photostability measurements of CNDs with 561 nm excitation under continuous higher intensity (0.3 kW/cm^2) confocal excitation (561 nm). Reproduced with permission of American Chemical Society from Ref. [114]. (c) Dual fluorescence bands observed in CNDs, which could be attributed to core- and surface-state emission. Reproduced with permission of American Chemical Society from Ref. [115]. (d) Three types of CDs with green emission chosen to clarify the surface-state PL mechanism. (e)–(f) The electronic state in CDs. (g) TA spectra for CDs 1–3 at 400 nm excitation. CDs 1: electrochemically synthesized CNDs, CDs 2: solvothermally synthesized GQDs 1, CDs 3: microwave-synthesized CNDs, GSB: ground-state bleaching, ESA: excited-state absorption, SE: stimulated emission. Reproduced with permission of American Chemical Society from Ref. [117].

Tang and co-workers pointed out that the dual PL bands of CNDs were attributed to core and surface-state emissions [115]. They conducted temperature-dependent fluorescence measurements and found that the dual emission bands exhibited similar temperature dependence (Fig. 10(c)). The strong electron–electron interactions and weak electron–phonon interactions could account for the very broad PL band, even at 77 K. Wen et al. indicated that the PL of CNDs consisted of two overlapping spectral bands, which were ascribed to the intrinsic and extrinsic states [116]. Band I originated from the localized sp^2 nanodomains, in which the energy band gap was determined by the size and shape of the domains with a small bandwidth of 175 meV. Band II originated from the surface states with a much broader bandwidth of 450 meV. A fast trapping process was observed from the nanodomains into the surface states, with a time constant of 400 fs. Relaxation with time constants of a few picoseconds, tens of picoseconds, and a few nanoseconds observed at each wavelength arose from the relaxation by optical phonon scattering, acoustic phonon scattering, and e–h recombination, respectively. The wavelength-dependent PL was attributed to the isolated and broadly distributed PL in the surface.

Furthermore, in our recent collaboration, the surface states for green emission of several CDs were confirmed. Three types of CDs (denoted as CDs 1–3) with different carbon structures and similar PL emissions were chosen as the model system (Figs. 10(d)–10(e)) [117]. CD-1 was synthesized by electrochemical ablation of graphite rod electrodes (top-down method), and they possessed high graphitic crystallinity [23]; CD-2 was fabricated by a two-step method combining "top-down" cutting of GO and various separation routes (a kind of GQD) [30]; CD-3 was synthesized by microwave-assisted small-molecule carbonization (bottom-up method) [118]. Femtosecond TA spectroscopy was used to shed light on the PL mechanism for these three samples at 400 nm excitation. From Fig. 10(g), despite the spectral superposition in each TA spectrum, it is still amazing that the transient features in the three types of carbon nanomaterials can be attributed to the same model. The main difference is the intensity of the stimulated emission. This result proved that all the investigated CDs had the same excited-state behaviors. The only difference was the proportion of radiative recombination during the whole relaxation process of the photogenerated carriers. It is considered that the degree of carbon crystallization decreased, whereas the QYs increased for CDs 1–3. The common photophysics unraveled: the photogenerated carriers are first stored in the carbon backbone. They then leak quickly into any possible emission state (the hybridization structure of the carbon backbone and chemical groups) and trap (meaningless structures), in which graphitic crystallinity acts as a temporary reservoir (Fig. 10(f)). In this mechanism, the increased degree of graphitic crystallinity or carbonization will lead to better photostability but lower the QY because of different non-radiative relaxation channels created by the carbon structures (for example, the interlamination of the graphite). Furthermore, because the green PL can be translated to blue by chemical reduction (–COOH changes to –OH) and the green PL is quenched at high or low pH ranges (protonation/deprotonation of carboxyl groups), the surface state can be attributed to the special molecule conformations consisting of these oxygen-based groups and several edge carbon atoms of the carbon backbone. Also, owing to the variety of possible edge states, some edge states could be non-radiative states (traps). Hence, the competition among different emission centers and traps dominates the optical properties of carbon nanomaterials. The fact that the CDs used contained both GQDs and CNDs explains how the surface states could be common and similar for both GQDs and CNDs [41, 56, 90, 96, 119, 120].

Although the origin of fluorescence in CNDs is not yet entirely understood, there is mounting evidence that emission arises from both an intrinsic band gap resulting from confined sp^2 conjugation in the core of CNDs and extrinsic fluorescence resulting from a surface state that can be either directly excited or excited by energy transfer from an intrinsic band. As a result, the tunable fluorescence emission of CDs can be achieved by either controlling the domain size of sp^2 conjugation or modifying the chemical groups formed on the surfaces of CNDs.

5.3 Molecule state and carbon-core state in CNDs

First of all, the difference between the surface and molecule state should be noted. As mentioned above, the surface state is the PL center, formed by the synergetic hybridization of the chemical groups and the carbon core, whereas the molecule state is the PL center formed solely by an organic fluorophore; the fluorophore is connected on the surface or interior of the carbon backbone and can exhibit PL emission directly. The molecule state is the emerging PL center for a type of CND prepared by small-molecule carbonization (bottom-up route). To prepare these CNDs, small fluorophore molecules are formed at low reaction temperatures. As the carbonization temperature increases, the carbon core is formed by dehydration of the initial molecules or consumption of the formed fluorophores. These CNDs exhibit strong PL emission with high QYs, whereas the carbon-core state possesses weak PL behavior with high photostability.

Giannelis and co-workers first investigated the formation mechanism of CNDs with both the molecule and carbon-core states (Fig. 11(a)) [121]. Using citric acid (CA) and ethanolamine (EA) as the model system, pyrolysis at 180 °C resulted in a molecular precursor

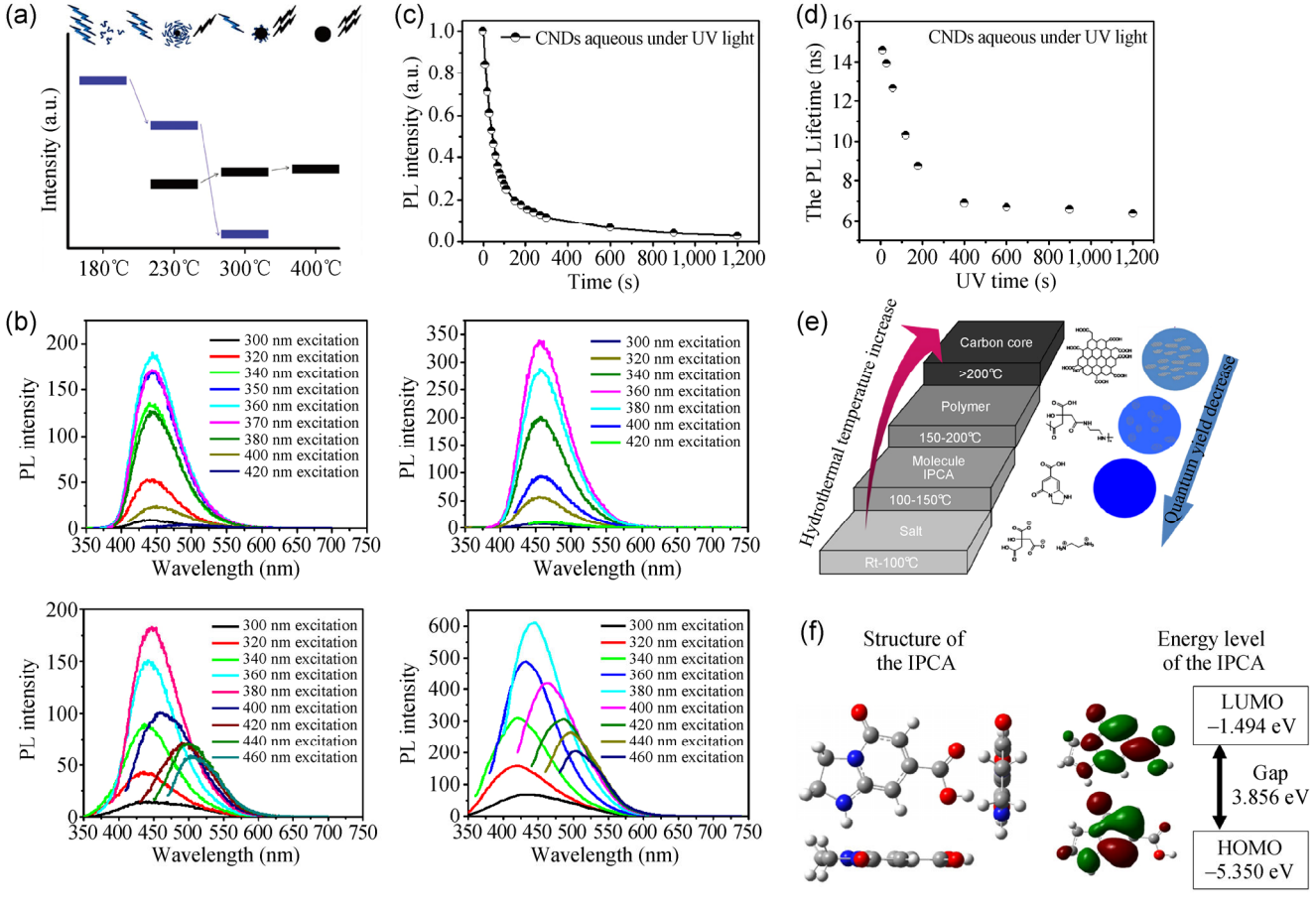

Figure 11 Molecule state and carbon-core state in CNDs. (a) Schematic representation of the emission characteristics of three photoactive species produced from the thermal treatment of a mixture of CA and EA. During pyrolysis, the organic fluorophores (blue groups) are consumed for the buildup of the carbogenic core (black sphere) so that the PL component that corresponds to the carbogenic core (black bars) increases at the expenses of the component that arises from the organic fluorophores (blue bars). Reproduced with permission of American Chemical Society from Ref. [121]. (b) The excitation-dependent PL for CNDs 1–4 (from left to right) prepared from CA and EDA at different temperature. Reproduced with permission of Wiley-VCH from Ref. [65]. (c) The PL intensity of CNDs as a function of high-power UV exposure time. (d) The PL lifetime of CNDs as a function of UV exposure time Reproduced with permission of Royal Society of Chemistry from Ref. [122]. (e) The suggested product of CA and EDA at different temperatures. (f) The determined molecule structure of the fluorophore.

with a strongly intense PL and high QY of 50%. At higher temperatures (230 ℃), a carbogenic core started forming, and the PL was due to the presence of both molecular fluorophores and the carbogenic core. However, the QY for these CNDs was only 15%. This value is significantly lower than the abovementioned 50%, which suggests that a large number of fluorophores were used as the building blocks of the carbogenic domains. CNPs that exhibited PL mostly or exclusively arising from carbogenic cores were obtained at even higher temperatures (300 and 400 ℃), and the QY decreased markedly. The quenching of the carbon-core structure to facilitate the emission of the neighboring molecule state might also account to some extent for the suppressed emission of the PL center observed for CNPs prepared at high temperature.

Yang and co-workers also investigated the molecule and carbon-core states using CA and ethylenediamine (EDA) as model molecules. They prepared four kinds of CNDs at 150, 200, 250, and 300 ℃ (denoted as CNDs 1–4) [65]. CNDs prepared below 250 ℃ always have difficulty in TEM imaging, perhaps owing to the unshaped nanoparticles, especially at low synthesis temperatures. The QYs of CNDs 1–4 decreased, whereas the photostability increased, and the excitation-dependent PL was increasingly obvious (Fig. 11(b)). Furthermore, the PL intensity of CND 2 was quenched over 90% by high-power UV exposure (the generated ·OH with ultrahigh oxidation potential can destroy the molecule state of CNDs), as shown in Fig. 11(c) [122]. However, the PL lifetime decreased and was maintained at ca. 6 ns (Fig. 11(d)), which corresponded to the carbon-core state with strong photostability and weak PL. Based on these results, Fig. 11(e) summarizes the rules for CND formation and the PL mechanism. At reaction temperatures less than 150 ℃, a type of fluorophore with a high QY was formed. At reaction temperatures of 150–250 ℃, CA and EDA formed both the fluorophore molecules and the crosslinked polymer backbone. In the meantime, CNDs were formed by the dehydration of CA and EDA. In this situation, the PL mainly results from the formed fluorophores connected on the CNDs. At high temperatures (over 300 ℃), owing to further carbonization, partial fluorophores are consumed to further form the carbon core, and the PL is due to the synergistic effect of the carbogenic core and the molecule state. In the latest research, the authors purified and confirmed the structure of a fluorophore molecule prepared at temperatures lower than 150 ℃ (Fig. 11(f)).

6 PL mechanism of PDs: the crosslink-enhanced emission (CEE) effect

Non-conjugated PDs, which are a specific type of CDs, possess aggregated polymer structures and have drawn increasing attention over the last three years [13–15, 104, 123–125]. These types of PDs are different from the conjugated PDs, which are obtained from an assembly of fluorescent-conjugated polymers [126]. The PDs under discussion here are always prepared from non-conjugated polymers by dehydration, condensation, carbonization, or assembly routes. In these situations, the PL centers are attributed to the formed carbon core or the fluorophores. Owing to convenient surface modification, PDs are very promising as novel fluorescent materials. To extend the application of these types of materials, it is highly important to confirm a clear PL mechanism. In several pioneering works, PL behaviors were preliminary investigated for several types of PDs. Liu et al. synthesized PDs by a grass hydrothermal route [13]. Dai and co-workers prepared PDs by polymerizing carbon tetrachloride and ethylenediamine [14]. Zhu et al. used a general route to transform linear non-conjugated polymers into fluorescent PDs [15]. With these types of materials, the formation of polymer aggregations (i.e., PDs) promoted the PL behavior [15, 127].

The clear PL mechanism of PDs was clarified to be the CEE effect by Yang's group [55]. The PL properties of potential fluorescent centers (fluorophores) are amplified by the CEE effect. Using branched PEI as a model non-conjugated polymer, the CEE effect was investigated for a series of PEI-based PDs (PDs 1–4). The PEI-based PDs possessed potential fluorophores (secondary and tertiary amines), and the enhanced PL originated from the decreased vibration and rotation in such crosslinked PEI-based PDs. Figures 12(a)–12(b) show the applied crosslinked PDs and their PL properties. The PDs possessed temperature-dependent PL (Fig. 12(c)); high temperatures quenched the PL to

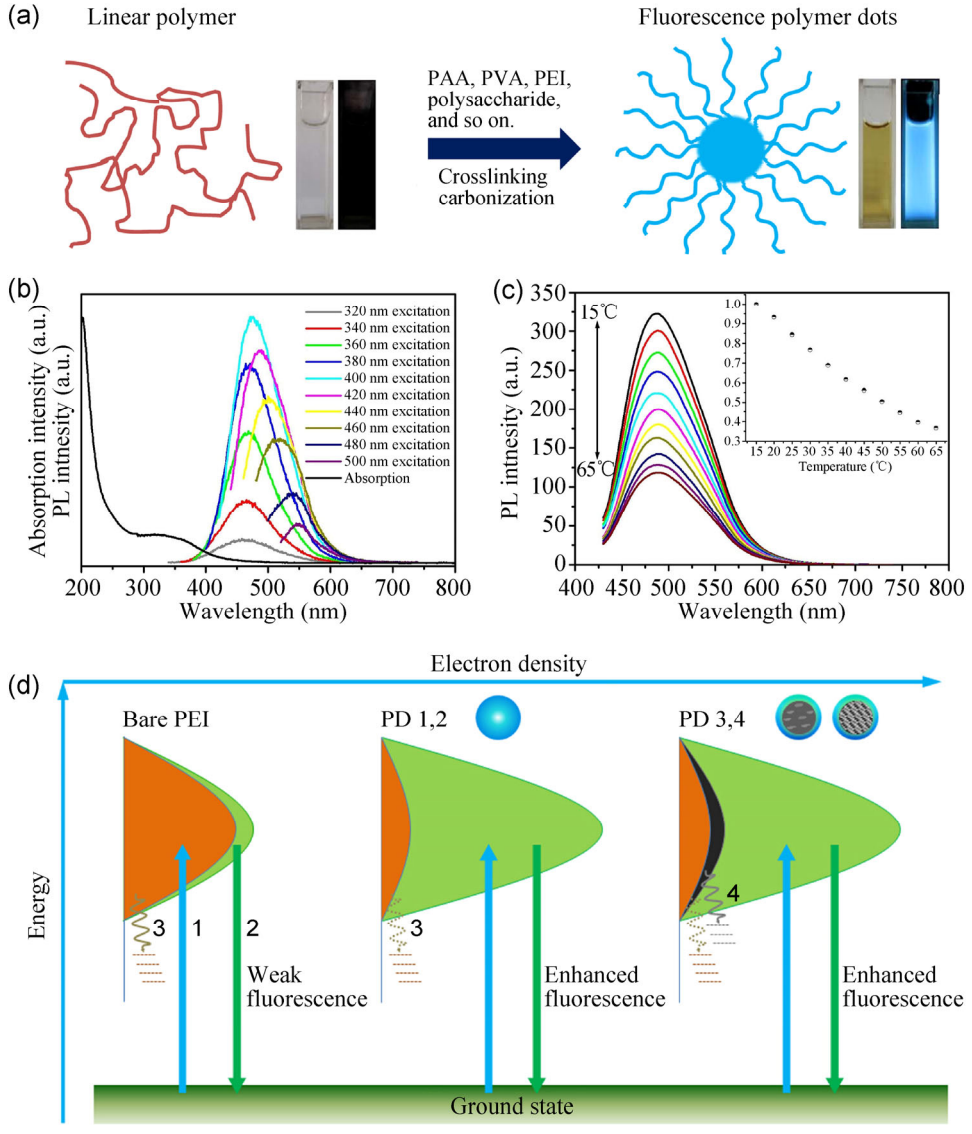

Figure 12 PL mechanism of PDs: the crosslinking-enhanced emission (CEE) effect. (a) Scheme of the preparation process of non-conjugated PDs. Reproduced with permission of Royal Society of Chemistry from Ref. [15]. (b) The absorption and fluorescence spectra of crosslinking PDs. (c) The temperature-dependent PL of PDs. (d) Representation for the PL mechanism (CEE effect) of bare PEI and PDs 1–4. (1) Electrons excited from the ground state and trapped by the amino-based states; (2) excited electrons return to the ground state via the radiative route; (3) excited electrons return to the ground state via a vibration and rotation non-radiative route; (4) excited electrons return to the ground state via a carbon core-based non-radiative route. Reproduced with permission of Royal Society of Chemistry from Ref. [55].

some degree. This behavior preliminary proved that the crosslinked skeleton decreases the vibration and rotation of the amine-based PL center in the PDs (the high temperature aggravates the vibration and rotation, thus increasing the non-radiative process). The electron level of PEI and the PEI PDs is shown in Fig. 12(d). For bare PEI, the excited electrons mainly dropped to the ground state through a non-radiative vibration/ rotation process. For PDs 1 and 2, owing to the crosslinked skeleton, the vibration and rotation of the amino-based fluorophores were restricted, and the percentage of radiative process increased (CEE effect). For PD 3, the PEI chains were immobilized by the amorphous carbon core; both the immobilization of the PEI chains and the antenna effect of the carbon core enhanced the PL. For PD 4, although the PEI

chains were fixed and the amine-based center was enhanced by the CEE effect, the carbon core with its multilayer crystal lattice possessed non-radiative structures and traps. As a result, the radiative process was neutralized and confined.

Actually, previous work has confirmed the CEE effect, but the authors did not realize such an important PL enhancement principle. For example, Sun and co-workers reported the fabrication of ultra-bright amphiphilic PDs by the self-assembly of a segmented copolymer [125]. They demonstrated that the rigid and compact structure of the PDs played a crucial role in the excitation-dependent and enhanced fluorescence behavior. The pH-dependent fluorescence of PDs further confirms that an acidic environment results in a much more rigid and compact conforma tion and induces the unique fluorescent effect.

Furthermore, the concept of non-conjugated PDs was very different with the dendrimers (such as Poly (amido amine)s, PAMAMs). Dendrimers always possess a sphere-like shape, and they are typified by an internal molecular architecture consisting of tree-like branching, with each outward layer or generation containing exponentially more branching points [128, 129]. In general, non-conjugated PDs include these types of materials, and possessed the most extensive concept in all of the PDs. The concept of the CEE effect is also different from the reported aggregation-induced emission (AIE), which mainly refers to small organic molecules exhibiting physical or supramolecular aggregation [130, 131].

7 Summary and outlook

In this review, we have briefly introduced the category, synthesis methods, and properties of three CD materials (GQDs, CNDs, and PDs), and we have described recent advances in elucidating the PL mechanism of these materials. A wide range of approaches (top-down cutting and bottom-up carbonization) already exist for producing CDs with controllable characteristics. Investigation of the PL properties of CDs includes the different emission centers, excitation dependence, and pH and solvent sensitivity, all of which are hot research topics. Although a variety of CDs with different chemical structures have been developed, four respectable PL principles have been elucidated: the quantum confinement effect or conjugated π-domains, which are determined by the carbon core; the surface state, which is determined by hybridization of the carbon backbone and connected chemical groups; the molecule state, which is determined solely by the fluorescent molecules connected on the surface or interior of the CDs; and the CEE effect.

We would like to share our perspectives on some critical issues regarding the PL mechanism and possible solutions to potentially address these issues. There are three main challenges. First, it is still a great challenge to develop an efficient method for mass production of high-quality CDs. Because of their "uncertain" chemical groups on the surface, the CDs are types of "uncertain" materials. If the chemical structure of CDs can be controlled during the synthesis process, it will be convenient and possible to provide a definite PL mechanism for CDs. Second, researchers should apply sufficient characterization to illuminate the PL center or PL mechanism. Owing to inadequate investigation, the PL center for many reported CDs has been blurred or even mistaken. And last, it would be very useful to study different CDs together for systematic comparison. Although the diversity of existing CDs increases the difficulty of systematic research, the PL mechanism is similar for these types of CDs.

Owing to the outstanding properties of fluorescent carbon materials, such as superior fluorescence, physiological stability, pH sensitivity, fine biocom-patibility, and low toxicity, they are being exploited for energy-related devices, composites materials, and environmental and biological applications. For example, the storage and transport of electrons in CDs have been exploited for solar cells [42, 132, 133], organic light-emitting diodes (OLEDs) [50, 134], photodetectors [135], photocatalysts [23], and supercapacitors [136]. The quench-based PL (on-off and off-on) of CDs has been developed in sensors for biomolecules, metal ions, and toxic/dangerous substances [74, 137–138]. The stable PL and low toxicity of CDs make them a perfect candidate for bio-imaging [30, 53], biosensors [139], drug delivery [140], and medical diagnosis [141]. The rich chemical groups on the surfaces and facile modification of CDs are beneficial for fluorescent

nanocomposites [127], functional hybrids [142], and high-refractive-index materials [143]. In the future, we expect the advent of more facile and robust synthetic methods and novel applications to better realize the increasing potential of CD materials. Moreover, the synthesis process, the CDs themselves, and their application is thought to be safe and environmentally benign, which shows the powerful potential of these materials for the abovementioned applications. For all these reasons, it is extremely important to promote the development of CDs, which could be a promising candidate to replace organic dyes or inorganic quantum dots in related fields. Rapid developments in synthesizing CDs with controllable sizes, tailorable chemical structures, and a clear PL mechanism will promote their application.

Acknowledgements

This work was supported by the National Science Foundation of China (Grand Nos. 51373065, 21221063, 81320108011, 91123031), the National Basic Research Program of China (973 Program, Grant No. 2012CB933800), and the Specialized Research Fund for the Doctoral Program of Higher Education (No. 20130061130010).

References

[1] Baker, S. N.; Baker, G. A. Luminescent carbon nanodots: Emergent nanolights. *Angew. Chem. Int. Ed.* **2010**, *49*, 6726–6744.

[2] Li, H. T.; Kang, Z. H.; Liu, Y.; Lee, S.-T. Carbon nanodots: Synthesis, properties and applications. *J. Mater. Chem.* **2012**, *22*, 24230–24253.

[3] Welsher, K.; Liu, Z.; Sherlock, S. P.; Robinson, J. T.; Chen, Z.; Daranciang, D.; Dai, H. J. A route to brightly fluorescent carbon nanotubes for near-infrared imaging in mice. *Nat. Nanotechol.* **2009**, *4*, 773–780.

[4] Gokus, T.; Nair, R. R.; Bonetti, A.; Bohmler, M.; Lombardo, A.; Novoselov, K. S.; Geim, A. K.; Ferrari, A. C.; Hartschuh, A. Making graphene luminescent by oxygen plasma treatment. *ACS Nano* **2009**, *3*, 3963–3968.

[5] Eda, G.; Lin, Y.-Y.; Mattevi, C.; Yamaguchi, H.; Chen, H.-A.; Chen, I.-S.; Chen, C.-W.; Chhowalla, M. Blue photoluminescence from chemically derived graphene oxide. *Adv. Mater.* **2010**, *22*, 505–509.

[6] Zhu, S. J.; Tang, S. J.; Zhang, J. H.; Yang, B. Control the size and surface chemistry of graphene for the rising fluorescent materials. *Chem. Commun.* **2012**, *48*, 4527–4539.

[7] Shen, J. H.; Zhu, Y. H.; Yang, X. L.; Li, C. Z. Graphene quantum dots: emergent nanolights for bioimaging, sensors, catalysis and photovoltaic devices. *Chem. Commun.* **2012**, *48*, 3686–3699.

[8] Zhang, Z. P.; Zhang, J.; Chen, N.; Qu, L. T. Graphene quantum dots: An emerging material for energy-related applications and beyond. *Energy Environ. Sci.* **2012**, *5*, 8869–8890.

[9] Li, L. L.; Wu, G. H.; Yang, G. H.; Peng, J.; Zhao, J. W.; Zhu, J.-J. Focusing on luminescent graphene quantum dots: Current status and future perspectives. *Nanoscale* **2013**, *5*, 4015–4039.

[10] Bacon, M.; Bradley, S. J.; Nann, T. Graphene quantum dots. *Part. Part. Syst. Charact.* **2014**, *31*, 415–428.

[11] Zhou, X. J.; Guo, S. W.; Zhang, J. Y. Solution-processable graphene quantum dots. *ChemPhysChem* **2013**, *14*, 2627–2640.

[12] Lin, L. P.; Rong, M. C.; Luo, F.; Chen, D. M.; Wang, Y. R.; Chen, X. Luminescent graphene quantum dots as new fluorescent materials for environmental and biological applications. *TrAC Trends Anal. Chem.* **2014**, *54*, 83–102.

[13] Liu, S.; Tian, J. Q.; Wang, L.; Zhang, Y. W.; Qin, X. Y.; Luo, Y. L.; Asiri, A. M.; Al-Youbi, A. O.; Sun, X. P. Hydrothermal treatment of grass: A low-cost, green route to nitrogen-doped, carbon-rich, photoluminescent polymer nanodots as an effective fluorescent sensing platform for label-free detection of Cu(II) ions. *Adv. Mater.* **2012**, *24*, 2037–2041.

[14] Qiao, Z.-A.; Huo, Q. S.; Chi, M. F.; Veith, G. M.; Binder, A. J.; Dai, S. A "ship-in-a-bottle" approach to synthesis of polymer dots@silica or polymer dots@carbon core-shell nanospheres. *Adv. Mater.* **2012**, *24*, 6017–6021.

[15] Zhu, S. J.; Zhang, J. H; Wang, L.; Song, Y. B.; Zhang, G. Y.; Wang, H. Y.; Yang, B. A general route to make non-conjugated linear polymers luminescent. *Chem. Commun.* **2012**, *48*, 10889–10891.

[16] Yu, S.-J.; Kang, M.-W.; Chang, H.-C.; Chen, K.-M.; Yu, Y.-C. Bright fluorescent nanodiamonds: No photobleaching and low cytotoxicity. *J. Am. Chem. Soc.* **2005**, *127*, 17604–17605.

[17] Mochalin, V. N.; Shenderova, O.; Ho, D.; Gogotsi, Y. The properties and applications of nanodiamonds. *Nat. Nanotechnol.* **2012**, *7*, 11–23.

[18] Cao, L.; Meziani, M. J.; Sahu, S.; Sun, Y.-P. Photoluminescence properties of graphene versus other carbon nanomaterials. *Acc. Chem. Res.* **2013**, *46*, 171–180.

[19] Song, Y. B.; Zhu, S. J.; Yang, B. Bioimaging based on fluorescent carbon dots. *RSC Adv.* **2014**, *4*, 27184–27200.

[20] Feng, X. L.; Wu, J. S.; Ai, M.; Pisula, W.; Zhi, L. J.; Rabe, J. P.; Müllen, K. Triangle-shaped polycyclic aromatic hydrocarbons. *Angew. Chem. Int. Ed.* **2007**, *46*, 3033–3036.

[21] Yan, X.; Cui, X.; Li, L.-S. Synthesis of large, stable colloidal graphene quantum dots with tunable size. *J. Am. Chem. Soc.* **2010**, *132*, 5944–5945.

[22] Qiao, Z.-A.; Wang, Y. F.; Gao, Y.; Li, H. W.; Dai, T. Y.; Liu, Y. L.; Huo, Q. S. Commercially activated carbon as the source for producing multicolor photoluminescent carbon dots by chemical oxidation. *Chem. Commun.* **2010**, *46*, 8812–8814.

[23] Li, H. T.; He, X. D.; Kang, Z. H.; Huang, H.; Liu, Y.; Liu, J. L.; Lian, S. Y.; Tsang, C. H.; Yang, X. B.; Lee, S.-T. Water-soluble fluorescent carbon quantum dots and photocatalyst design. *Angew. Chem. Int. Ed.* **2010**, *49*, 4430–4434.

[24] Peng, J.; Gao, W.; Gupta, B. K.; Liu, Z.; Romero-Aburto, R.; Ge, L. H.; Song, L. H.; Alemany, L. B.; Zhan, X. B.; Gao, G. H. et al. Graphene quantum dots derived from carbon fibers. *Nano Lett.* **2012**, *12*, 844–849.

[25] Xu, X.Y.; Ray, R.; Gu, Y. L.; Ploehn, H. J.; Gearheart, L.; Raker, K.; Scrivens, W. A. Electrophoretic analysis and purification of fluorescent single-walled carbon nanotube fragments. *J. Am. Chem. Soc.* **2004**, *126*, 12736–12737.

[26] Shinde, D. B.; Pillai, V. K. Electrochemical preparation of luminescent graphene quantum dots from multiwalled carbon nanotubes. *Chem.-Eur. J.* **2012**, *18*, 12522–12528.

[27] Dong, Y. Q.; Chen, C. Q.; Zheng, X. T.; Gao, L. L.; Cui, Z. M.; Yang, H. B.; Guo, C. X.; Chi, Y. W.; Li, C. M. One-step and high yield simultaneous preparation of single- and multi-layer graphene quantum dots from CX-72 carbon black. *J. Mater. Chem.* **2012**, *22*, 8764–8766.

[28] Liu, H. P.; Ye, T.; Mao, C. D. Fluorescent carbon nanoparticles derived from candle soot. *Angew. Chem. Int. Ed.* **2007**, *46*, 6473–6475.

[29] Tao, H. Q.; Yang, K.; Ma, Z.; Wan, J. M.; Zhang, Y. J.; Kang, Z. H.; Liu, Z. In vivo NIR fluorescence imaging, biodistribution, and toxicology of photoluminescent carbon dots produced from carbon nanotubes and graphite. *Small* **2012**, *8*, 281–290.

[30] Zhu, S. J.; Zhang, J. H.; Qiao, C. Y.; Tang, S. J.; Li, Y. F.; Yuan, W. J.; Li, B.; Tian, L.; Liu, F.; Hu, R. et al. Strongly green-photoluminescent graphene quantum dots for bioimaging applications. *Chem. Commun.* **2011**, *47*, 6858–6860.

[31] Zhu, S. J.; Zhang, J. H.; Liu, X.; Li, B.; Wang, X. F.; Tang, S. J.; Meng, Q. N.; Li, Y. F.; Shi, C.; Hu, R. et al. Graphene quantum dots with controllable surface oxidation, tunable fluorescence and up-conversion emission. *RSC Adv.* **2012**, *2*, 2717–2720.

[32] Lu, J.; Yang, J.-X.; Wang, J. Z.; Lim, A.; Wang, S.; Loh, K. P. One-pot synthesis of fluorescent carbon nanoribbons, nanoparticles, and graphene by the exfoliation of graphite in ionic liquids. *ACS Nano* **2009**, *3*, 2367–2375.

[33] Zheng, L. Y.; Chi, Y. W.; Dong, Y. Q.; Lin, J. P.; Wang, B. B. Electrochemiluminescence of water-soluble carbon nanocrystals released electrochemically from graphite. *J. Am. Chem. Soc.* **2009**, *131*, 4564–4565.

[34] Pan, D. Y.; Zhang, J. C.; Li, Z.; Wu, M. H. Hydrothermal route for cutting graphene sheets into blue-luminescent graphene quantum dots. *Adv. Mater.* **2010**, *22*, 734–738.

[35] Lin, L. X.; Zhang, S. W. Creating high yield water soluble luminescent graphene quantum dots via exfoliating and disintegrating carbon nanotubes and graphite flakes. *Chem. Commun.* **2012**, *48*, 10177–10179.

[36] Bottini, M.; Balasubramanian, C.; Dawson, M. I.; Bergamaschi, A.; Bellucci, S.; Mustelin, T. Isolation and characterization of fluorescent nanoparticles from pristine and oxidized electric arc-produced single-walled carbon nanotubes. *J. Phys.Chem. B* **2006**, *110*, 831–836.

[37] Sun, Y.-P.; Zhou, B.; Lin, Y.; Wang, W.; Fernando, K. A.; Pathak, P.; Meziani, M. J.; Harruff, B. A.; Wang, X.; Wang, H. F. et al. Quantum-sized carbon dots for bright and colorful photoluminescence. *J. Am. Chem. Soc.* **2006**, *128*, 7756–7757.

[38] Lee, J.; Kim, K.; Park, W. I.; Kim, B.-H.; Park, J. H.; Kim, T.-H.; Bong, S.; Kim, C.-H.; Chae, G.; Jun, M. et al. Uniform graphene quantum dots patterned from self-assembled silica nanodots. *Nano Lett.* **2012**, *12*, 6078–6083.

[39] Fan, L. L.; Zhu, M.; Lee, X.; Zhang, R. J.; Wang, K. L.; Wei, J. Q.; Zhong, M. L.; Wu, D. H.; Zhu, H. W. Direct synthesis of graphene quantum dots by chemical vapor deposition. *Part. Part. Syst. Charact.* **2013**, *30*, 764–769.

[40] Zhao, Q.-L.; Zhang, Z.-L.; Huang, B.-H.; Peng, J.; Zhang, M.; Pang, D.-W. Facile preparation of low cytotoxicity fluorescent carbon nanocrystals by electrooxidation of graphite. *Chem. Commun.* **2008**, 5116–5118.

[41] Bao, L.; Zhang, Z.-L.; Tian, Z.-Q.; Zhang, L.; Liu, C.; Lin, Y.; Qi, B. P.; Pang, D.-W. Electrochemical tuning of luminescent carbon nanodots: From preparation to luminescence mechanism. *Adv. Mater.* **2011**, *23*, 5801–5806.

[42] Li, Y.; Hu, Y.; Zhao, Y.; Shi, G. Q.; Deng, L. E.; Hou, Y. B.; Qu, L. T. An electrochemical avenue to green-luminescent graphene quantum dots as potential electron-acceptors for photovoltaics. *Adv. Mater.* **2011**, *23*, 776–780.

[43] Deng, J. H.; Lu, Q. J.; Mi, N. X.; Li, H. T.; Liu, M. L.; Xu, M. C.; Tan, L.; Xie, Q. J.; Zhang, Y. Y.; Yao, S. Z. Electrochemical synthesis of carbon nanodots directly from alcohols. *Chem.-Eur. J.* **2014**, *20*, 4993–4999.

[44] Zhou, X. J.; Zhang, Y.; Wang, C.; Wu, X. C.; Yang, Y. Q.; Zheng, B.; Wu, H. X.; Guo, S. W.; Zhang, J. Y. Photo-Fenton reaction of graphene oxide: a new strategy to prepare graphene quantum dots for DNA cleavage. *ACS Nano* **2012**, *6*, 6592–6599.

[45] Yang, Z.-C.; Wang, M.; Yong, A. M.; Wong, S. Y.; Zhang, X.-H.; Tan, H.; Chang, A. Y.; Li, X.; Wang, J. Intrinsically fluorescent carbon dots with tunable emission derived from hydrothermal treatment of glucose in the presence of monopotassium phosphate. *Chem. Commun.* **2011**, *47*, 11615–11617.

[46] Zhu, H.; Wang, X. L.; Li, Y. L.; Wang, Z. J.; Yang, F.; Yang, X. R. Microwave synthesis of fluorescent carbon nanoparticles with electrochemiluminescence properties. *Chem. Commun.* **2009**, 5118–5120.

[47] Bourlinos, A. B.; Stassinopoulos, A.; Anglos, D.; Zboril, R.; Karakassides, M.; Giannelis, E. P. Surface functionalized carbogenic quantum dots. *Small* **2008**, *4*, 455–458.

[48] Peng, H.; Travas-Sejdic, J. Simple aqueous solution route to luminescent carbogenic dots from carbohydrates. *Chem. Mater.* **2009**, *21*, 5563–5565.

[49] Zong, J.; Zhu, Y. H.; Yang, X. L.; Shen, J. H.; Li, C. Z. Synthesis of photoluminescent carbogenic dots using mesoporous silica spheres as nanoreactors. *Chem. Commun.* **2011**, *47*, 764–766.

[50] Tang, L. B.; Ji, R. B.; Cao, X. K.; Lin, J. Y.; Jiang, H. X.; Li, X. M.; Teng, K. S.; Luk, C. M.; Zeng, S. J.; Hao, J. H. et al. Deep ultraviolet photoluminescence of water-soluble self-passivated graphene quantum dots. *ACS Nano* **2012**, *6*, 5102–5110.

[51] Wang, J.; Wang, C.-F.; Chen, S. Amphiphilic egg-derived carbon dots: Rapid plasma fabrication, pyrolysis process, and multicolor printing patterns. *Angew. Chem. Int. Ed.* **2012**, *51*, 9297–9301.

[52] Zhang, C.; Liu, Y.; Xiong, X.-Q.; Peng, L.-H.; Gan, L.; Chen, C.-F.; Xu, H.-B. Three-dimensional nanographene based on triptycene: Synthesis and its application in fluorescence imaging. *Org. Lett.* **2012**, *14*, 5912–5915.

[53] Cao, L.; Wang, X.; Meziani, M. J.; Lu, F. S.; Wang, H. F.; Luo, P. J. G.; Lin, Y.; Harruff, B. A.; Veca, L. M.; Murray, D.; Xie, S.-Y.; Sun, Y.-P. Carbon dots for multiphoton bioimaging. *J. Am. Chem. Soc.* **2007**, *129*, 11318–11319.

[54] Shen, J. H.; Zhu, Y. H.; Chen, C.; Yang, X. L.; Li, C. Z. Facile preparation and upconversion luminescence of graphene quantum dots. *Chem. Commun.* **2011**, *47*, 2580–2582.

[55] Zhu, S. J.; Wang, L.; Zhou, N.; Zhao, X. H.; Song, Y. B.; Maharjan, S.; Zhang, J. H.; Lu, L. J.; Wang, H. Y.; Yang, B. The crosslink enhanced emission (CEE) in non-conjugated polymer dots: From the photoluminescence mechanism to the cellular uptake mechanism and internalization. *Chem. Commun.* **2014**, *50*, 13845–13848.

[56] Zheng, H. Z.; Wang, Q. L.; Long, Y. J.; Zhang, H. J.; Huang, X. X.; Zhu, R. Enhancing the luminescence of carbon dots with a reduction pathway. *Chem. Commun.* **2011**, *47*, 10650–10652.

[57] Nie, H.; Li, M. J.; Li, Q. S.; Liang, S. J.; Tan, Y. Y.; Sheng, L.; Shi, W.; Zhang, S. X.-A. Carbon dots with continuously tunable full-color emission and their application in ratiometric pH sensing. *Chem. Mater.* **2014**, *26*, 3104–3112.

[58] Tetsuka, H.; Asahi, R.; Nagoya, A.; Okamoto, K.; Tajima, I.; Ohta, R.; Okamoto, A. Optically tunable amino-functionalized graphene quantum dots. *Adv. Mater.* **2012**, *24*, 5333–5338.

[59] Wang, Y.; Kalytchuk, S.; Zhang, Y.; Shi, H. C.; Kershaw, S. V.; Rogach, A. L. Thickness-dependent full-color emission tunability in a flexible carbon dot ionogel. *J. Phys. Chem. Lett.* **2014**, *5*, 1412–1420.

[60] Wang, Y. Y.; Li, Y.; Yan, Y.; Xu, J.; Guan, B. Y.; Wang, Q.; Li, J. Y.; Yu, J. H. Luminescent carbon dots in a new magnesium aluminophosphate zeolite. *Chem. Commun.* **2013**, *49*, 9006–9008.

[61] Ray, S. C.; Saha, A.; Jana, N. R.; Sarkar, R. Fluorescent carbon nanoparticles: Synthesis, characterization, and bioimaging application. *J. Phys. Chem. C* **2009**, *113*, 18546–18551.

[62] Wang, X. H.; Qu, K. G.; Xu, B. L.; Ren, J. S.; Qu, X. G. Multicolor luminescent carbon nanoparticles: Synthesis, supramolecular assembly with porphyrin, intrinsic peroxidase-like catalytic activity and applications. *Nano Res.* **2011**, *4*, 908–920.

[63] Bhunia, S. K.; Saha, A.; Maity, A. R.; Ray, S. C.; Jana, N. R. Carbon nanoparticle-based fluorescent bioimaging probes. *Sci. Rep.* **2013**, *3*, 1473.

[64] Qu, D.; Zheng, M.; Zhang, L. G.; Zhao, H. F.; Xie, Z. G.; Jing, X. B.; Haddad, R. E.; Fan, H. Y.; Sun, Z. C. Formation mechanism and optimization of highly luminescent N-doped graphene quantum dots. *Sci. Rep.* **2014**, *4*, 5294.

[65] Zhu, S. J.; Meng, Q. N.; Wang, L.; Zhang, J. H.; Song, Y. B.; Jin, H.; Zhang, K.; Sun, H.; Wang, H. C.; Yang, B. Highly photoluminescent carbon dots for multicolor patterning, sensors, and bioimaging. *Angew. Chem. Int. Ed.* **2013**, *52*, 3953–3957.

[66] Gan, Z. X.; Wu, X. L.; Zhou, G. X.; Shen, J. C.; Chu, P. K. Is there real upconversion photoluminescence from graphene quantum dots? *Adv. Opt. Mater.* **2013**, *1*, 554–558.

[67] Wen, X. M.; Yu, P.; Toh, Y. R.; Ma, X. Q.; Tang, J. On the upconversion fluorescence in carbon nanodots and graphene quantum dots. *Chem. Commun.* **2014**, *50*, 4703–4706.

[68] Qu, S. N.; Liu, X. Y.; Guo, X. Y.; Chu, M. H.; Zhang, L. G.; Shen, D. Z. Amplified spontaneous green emission and

lasing emission from carbon nanoparticles. *Adv. Funct. Mater.* **2014**, *24*, 2689–2695.

[69] Fan, L. S.; Hu, Y. W.; Wang, X.; Zhang, L. L.; Li, F. H.; Han, D. X.; Li, Z. G.; Zhang, Q. X.; Wang, Z. X.; Niu, L. Fluorescence resonance energy transfer quenching at the surface of graphene quantum dots for ultrasensitive detection of TNT. *Talanta* **2012**, *101*, 192–197.

[70] Luo, P. J. G.; Sahu, S.; Yang, S.-T.; Sonkar, S. K.; Wang, J. P.; Wang, H. F.; LeCroy, G. E.; Cao, L.; Sun, Y.-P. Carbon "quantum" dots for optical bioimaging. *J. Mater. Chem. B* **2013**, *1*, 2116–2127.

[71] Esteves da Silva, J. C. G.; Gonçalves, H. M. R. Analytical and bioanalytical applications of carbon dots. *TrAC Trends Anal. Chem.* **2011**, *30*, 1327–1336.

[72] Sun, X. M.; Liu, Z.; Welsher, K.; Robinson, J. T.; Goodwin, A.; Zaric, S.; Dai, H. J. Nano-graphene oxide for cellular imaging and drug delivery. *Nano Res.* **2008**, *1*, 203–212.

[73] Goh, E. J.; Kim, K. S.; Kim, Y. R.; Jung, H. S.; Beack, S.; Kong, W. H.; Scarcelli, G.; Yun, S. H.; Hahn, S. K. Bioimaging of hyaluronic acid derivatives using nanosized carbon dots. *Biomacromolecules* **2012**, *13*, 2554–2561.

[74] Kong, B.; Zhu, A. W.; Ding, C. Q.; Zhao, X. M.; Li, B.; Tian, Y. Carbon dot-based inorganic-organic nanosystem for two-photon imaging and biosensing of pH variation in living cells and tissues. *Adv. Mater.* **2012**, *24*, 5844–5848.

[75] Liu, C. J.; Zhang, P.; Zhai, X. Y.; Tian, F.; Li, W. C.; Yang, J. H.; Liu, Y.; Wang, H. B.; Wang, W.; Liu, W. G. Nano-carrier for gene delivery and bioimaging based on carbon dots with PEI-passivation enhanced fluorescence. *Biomaterials* **2012**, *33*, 3604–3613.

[76] Nurunnabi, M.; Khatun, Z.; Huh, K. M.; Park, S. Y.; Lee, D. Y.; Cho, K. J.; Lee, Y. K. In vivo biodistribution and toxicology of carboxylated graphene quantum dots. *ACS Nano* **2013**, *7*, 6858–6867.

[77] Qian, J.; Wang, D.; Cai, F.-H.; Xi, W.; Peng, L.; Zhu, Z.-F.; He, H.; Hu, M.-L.; He, S. L. Observation of multiphoton-induced fluorescence from graphene oxide nanoparticles and applications in in vivo functional bioimaging. *Angew. Chem. Int. Ed.* **2012**, *51*, 10570–10575.

[78] Chien, C.-T.; Li, S.-S.; Lai, W.-J.; Yeh, Y.-C.; Chen, H.-A.; Chen, I.-S.; Chen, L.-C.; Chen, K.-H.; Nemoto, T.; Isoda, S. et al. Tunable photoluminescence from graphene oxide. *Angew. Chem. Int. Ed.* **2012**, *51*, 6662–6666.

[79] Luo, Z. T.; Vora, P. M.; Mele, E. J.; Johnson, A. T. C.; Kikkawa, J. M. Photoluminescence and band gap modulation in graphene oxide. *Appl. Phys. Lett.* **2009**, *94*, 111909.

[80] Galande, C.; Mohite, A. D.; Naumov, A. V.; Gao, W.; Ci, L. J.; Ajayan, A.; Gao, H.; Srivastava, A.; Weisman, R. B.; Ajayan, P. M. Quasi-molecular fluorescence from graphene oxide. *Sci. Rep.* **2011**, *1*, 85.

[81] Shang, J. Z.; Ma, L.; Li, J. W.; Ai, W.; Yu, T.; Gurzadyan, G. G. The origin of fluorescence from graphene oxide. *Sci. Rep.* **2012**, *2*, 792.

[82] Ritter, K. A.; Lyding, J. W. The influence of edge structure on the electronic properties of graphene quantum dots and nanoribbons. *Nat. Mater.* **2009**, *8*, 235–242.

[83] Radovic, L. R.; Bockrath, B. On the chemical nature of graphene edges: Origin of stability and potential for magnetism in carbon materials. *J. Am. Chem. Soc.* **2005**, *127*, 5917–5927.

[84] Xu, Q. F.; Zhou, Q.; Hua, Z.; Xue, Q.; Zhang, C. F.; Wang, X. Y.; Pan, D. Y.; Xiao, M. Single-particle spectroscopic measurements of fluorescent graphene quantum dots. *ACS Nano* **2013**, *7*, 10654–10661.

[85] Jin, S. H.; Kim, D. H.; Jun, G. H.; Hong, S. H.; Jeon, S. Tuning the photoluminescence of graphene quantum dots through the charge transfer effect of functional groups. *ACS Nano* **2013**, *7*, 1239–1245.

[86] Kumar, G. S.; Roy, R.; Sen, D.; Ghorai, U. K.; Thapa, R.; Mazumder, N.; Saha, S.; Chattopadhyay, K. K. Amino-functionalized graphene quantum dots: Origin of tunable heterogeneous photoluminescence. *Nanoscale* **2014**, *6*, 3384–3391.

[87] Qian, Z. S.; Ma, J. J.; Shan, X. Y.; Shao, L. X.; Zhou, J.; Chen, J. R.; Feng, H. Surface functionalization of graphene quantum dots with small organic molecules from photoluminescence modulation to bioimaging applications: An experimental and theoretical investigation. *RSC Adv.* **2013**, *3*, 14571–14579.

[88] Wang, L.; Wang, H.-Y.; Wang, Y.; Zhu, S.-J.; Zhang, Y.-L.; Zhang, J.-H.; Chen, Q.-D.; Han, W.; Xu, H.-L.; Yang, B. et al. Direct observation of quantum-confined graphene-like states and novel hybrid states in graphene oxide by transient spectroscopy. *Adv. Mater.* **2013**, *25*, 6539–6545.

[89] Wang, L.; Zhu, S.-J.; Wang, H.-Y.; Wang, Y.-F.; Hao, Y.-W.; Zhang, J.-H.; Chen, Q.-D.; Zhang, Y.-L.; Han, W.; Yang, B. et al. Unraveling bright molecule-like state and dark intrinsic state in green-fluorescence graphene quantum dots via ultrafast spectroscopy. *Adv. Opt. Mater.* **2013**, *1*, 264–271.

[90] Zhu, S. J.; Zhang, J. H.; Tang, S. J.; Qiao, C. Y.; Wang, L.; Wang, H. Y.; Liu, X.; Li, B.; Li, Y. F.; Yu, W. L. et al. Surface chemistry routes to modulate the photoluminescence of graphene quantum dots: From fluorescence mechanism to up-conversion bioimaging applications. *Adv. Funct. Mater.* **2012**, *22*, 4732–4740.

[91] Mei, Q. S.; Zhang, Z. P. Photoluminescent graphene oxide ink to print sensors onto microporous membranes for versatile visualization bioassays. *Angew. Chem. Int. Ed.* **2012**, *51*, 5602–5606.

[92] Liu, F.; Jang, M.-H.; Ha, H. D.; Kim, J. H.; Cho, Y.-H.; Seo, T. S. Facile synthetic method for pristine graphene quantum dots and graphene oxide quantum dots: Origin of blue and green luminescence. *Adv. Mater.* **2013**, *25*, 3657–3662.

[93] Li, X. M.; Lau, S. P.; Tang, L. B.; Ji, R. B.; Yang, P. Z. Multicolour light emission from chlorine-doped graphene quantum dots. *J. Mater. Chem. C* **2013**, *1*, 7308–7313.

[94] Luo, P. H.; Ji, Z.; Li, C.; Shi, G. Q. Aryl-modified graphene quantum dots with enhanced photoluminescence and improved pH tolerance. *Nanoscale* **2013**, *5*, 7361–7367.

[95] Sun, H. J.; Gao, N.; Wu, L.; Ren, J. S.; Wei, W. L.; Qu, X. G. Highly photoluminescent amino-functionalized graphene quantum dots used for sensing copper ions. *Chem.-Eur. J.* **2013**, *19*, 13362–13368.

[96] Feng, Y. Q.; Zhao, J. P.; Yan, X. B.; Tang, F. L.; Xue, Q. J. Enhancement in the fluorescence of graphene quantum dots by hydrazine hydrate reduction. *Carbon* **2014**, *66*, 334–339.

[97] Sun, Y. Q.; Wang, S. Q.; Li, C.; Luo, P. H.; Tao, L.; Wei, Y.; Shi, G. Q. Large scale preparation of graphene quantum dots from graphite with tunable fluorescence properties. *Phys. Chem. Chem. Phys.* **2013**, *15*, 9907–9913.

[98] Jiang, F.; Chen, D. Q.; Li, R. M.; Wang, Y. C.; Zhang, G. Q.; Li, S. M.; Zheng, J. P.; Huang, N. Y.; Gu, Y.; Wang, C. R. et al. Eco-friendly synthesis of size-controllable amine-functionalized graphene quantum dots with antimycoplasma properties. *Nanoscale* **2013**, *5*, 1137–1142.

[99] Lingam, K.; Podila, R.; Qian, H. J.; Serkiz, S.; Rao, A. M. Evidence for edge-state photoluminescence in graphene quantum dots. *Adv. Funct. Mater.* **2013**, *23*, 5062–5065.

[100] Chen, C.-F.; Park, C.-H.; Boudouris, B. W.; Horng, J.; Geng, B. S.; Girit, C.; Zettl, A.; Crommie, M. F.; Segalman, R. A.; Louie, S. G. et al. Controlling inelastic light scattering quantum pathways in graphene. *Nature* **2011**, *471*, 617–620.

[101] Li, L.-S.; Yan, X. Colloidal graphene quantum dots. *J. Phys. Chem. Lett.* **2010**, *1*, 2572–2576.

[102] Tomović, Z.; Watson, M. D.; Müllen, K. Superphenalene-based columnar liquid crystals. *Angew. Chem. Int. Ed.* **2004**, *43*, 755–758.

[103] Mueller, M. L.; Yan, X.; Dragnea, B.; Li, L.-S. Slow hot-carrier relaxation in colloidal graphene quantum dots. *Nano Lett.* **2011**, *11*, 56–60.

[104] Zhu, S. J.; Wang, L.; Li, B.; Song, Y. B.; Zhao, X. H.; Zhang, G. Y.; Zhang, S. T.; Lu, S. Y.; Zhang, J. H.; Wang, H. Y. et al. Investigation of photoluminescence mechanism of graphene quantum dots and evaluation of their assembly into polymer dots. *Carbon* **2014**, *77*, 462–472.

[105] Kim, S.; Hwang, S. W.; Kim, M.-K.; Shin, D. Y.; Shin, D. H.; Kim, C. O.; Yang, S. B.; Park, J. H.; Hwang, E.; Choi, S.-H. et al. Anomalous behaviors of visible luminescence from graphene quantum dots: Interplay between size and shape. *ACS Nano* **2012**, *6*, 8203–8208.

[106] Sk, M. A.; Ananthanarayanan, A.; Huang, L.; Lim, K. H.; Chen, P. Revealing the tunable photoluminescence properties of graphene quantum dots. *J. Mater. Chem. C* **2014**, *2*, 6954–6960.

[107] Lui, C. H.; Mak, K. F.; Shan, J.; Heinz, T. F. Ultrafast photoluminescence from graphene. *Phys. Rev. Lett.* **2010**, *105*, 127404.

[108] Kim, R.; Perebeinos, V.; Avouris, P. Relaxation of optically excited carriers in graphene. *Phys. Rev. B* **2011**, *84*, 075449.

[109] Fuyuno, N.; Kozawa, D.; Miyauchi, Y.; Mouri, S.; Kitaura, R.; Shinohara, H.; Yasuda, T.; Komatsu, N.; Matsuda, K. Drastic change in photoluminescence properties of graphene quantum dots by chromatographic separation. *Adv. Opt. Mater.* **2014**, *2*, 983–989.

[110] Tang, L. B.; Ji, R. B.; Li, X. M.; Teng, K. S.; Lau, S. P. Size-dependent structural and optical characteristics of glucose-derived graphene quantum dots. *Part. Part. Syst. Charact.* **2013**, *30*, 523–531.

[111] Kwon, W.; Rhee, S.-W. Facile synthesis of graphitic carbon quantum dots with size tunability and uniformity using reverse micelles. *Chem. Commun.* **2012**, *48*, 5256–5258.

[112] Kwon, W.; Lee, G.; Do, S.; Joo, T.; Rhee, S.-W. Size-controlled soft-template synthesis of carbon nanodots toward versatile photoactive materials. *Small* **2014**, *10*, 506–513.

[113] Wang, X.; Cao, L.; Yang, S.-T.; Lu, F. S.; Meziani, M. J.; Tian, L. L.; Sun, K. W.; Bloodgood, M. A.; Sun, Y.-P. Bandgap-like strong fluorescence in functionalized carbon nanoparticles. *Angew. Chem. Int. Ed.* **2010**, *49*, 5310–5314.

[114] Das, S. K.; Liu, Y. Y.; Yeom, S.; Kim, D. Y.; Richards, C. I. Single-particle fluorescence intensity fluctuations of carbon nanodots. *Nano Lett.* **2014**, *14*, 620–625.

[115] Yu, P.; Wen, X. M.; Toh, Y.-R.; Tang, J. Temperature-dependent fluorescence in carbon dots. *J. Phys. Chem. C* **2012**, *116*, 25552–25557.

[116] Wen, X. M.; Yu, P.; Toh, Y.-R.; Hao, X. T.; Tang, J. Intrinsic and extrinsic fluorescence in carbon nanodots: Ultrafast time-resolved fluorescence and carrier dynamics. *Adv. Opt. Mater.* **2013**, *1*, 173–178.

[117] Wang, L.; Zhu, S.-J.; Wang, H.-Y.; Qu, S.-N.; Zhang, Y.-L.; Zhang, J.-H.; Chen, Q.-D.; Xu, H.-L.; Han, W.; Yang, B. et al. Common origin of green luminescence in carbon nanodots and graphene quantum dots. *ACS Nano* **2014**, *8*, 2541–2547.

[118] Qu, S. N.; Wang, X. Y.; Lu, Q. P.; Liu, X. Y.; Wang, L. J. A biocompatible fluorescent ink based on water-soluble luminescent carbon nanodots. *Angew. Chem. Int. Ed.* **2012**, *51*, 12215–12218.

[119] Sun, H. J.; Wu, L.; Gao, N.; Ren, J. S.; Qu, X. G. Improvement of photoluminescence of graphene quantum dots with a biocompatible photochemical reduction pathway and its bioimaging application. *ACS Appl. Mater. Inter.* **2013**, *5*, 1174–1179.

[120] Li, L.-L.; Ji, J.; Fei, R.; Wang, C.-Z.; Lu, Q.; Zhang, J.-R.; Jiang, L.-P.; Zhu, J.-J. A facile microwave avenue to electrochemiluminescent two-color graphene quantum dots. *Adv. Funct. Mater.* **2012**, *22*, 2971–2979.

[121] Krysmann, M. J.; Kelarakis, A.; Dallas, P.; Giannelis, E. P. Formation mechanism of carbogenic nanoparticles with dual photoluminescence emission. *J. Am. Chem. Soc.* **2012**, *134*, 747–750.

[122] Song, Y. B.; Zhu, S. J.; Xiang, S. Y.; Zhao, X. H.; Zhang, J. H.; Zhang, H.; Fu, Y.; Yang, B. Investigation into the fluorescence quenching behaviors and applications of carbon dots. *Nanoscale* **2014**, *6*, 4676–4682.

[123] Ding, D.; Goh, C. C.; Feng, G. X.; Zhao, Z. J.; Liu, J.; Liu, R. R.; Tomczak, N.; Geng, J. L.; Tang, B. Z.; Ng, L. G.; et al. Ultrabright organic dots with aggregation-induced emission characteristics for real-time two-photon intravital vasculature imaging. *Adv. Mater.* **2013**, *25*, 6083–6088.

[124] Lai, T. T.; Zheng, E. H.; Chen, L. X.; Wang, X. Y.; Kong, L. C.; You, C. P.; Ruan, Y. M.; Weng, X. X. Hybrid carbon source for producing nitrogen-doped polymer nanodots: One-pot hydrothermal synthesis, fluorescence enhancement and highly selective detection of Fe(III). *Nanoscale* **2013**, *5*, 8015–8021.

[125] Sun, Y.; Cao, W. P.; Li, S. L.; Jin, S. B.; Hu, K. L.; Hu, L. M.; Huang, Y. Y.; Gao, X. Y.; Wu, Y.; Liang, X.-J. Ultrabright and multicolorful fluorescence of amphiphilic polyethyleneimine polymer dots for efficiently combined imaging and therapy. *Sci. Rep.* **2013**, *3*, 3036.

[126] Wu, C. F.; Chiu, D. T. Highly fluorescent semiconducting polymer dots for biology and medicine. *Angew. Chem. Int. Ed.* **2013**, *52*, 3086–3109.

[127] Zhu, S. J.; Zhang, J. H.; Song, Y. B.; Zhang, G. Y.; Zhang, H.; Yang, B. Fluorescent nanocomposite based on PVA polymer dots. *Acta Chim. Sinica* **2012**, *70*, 2311–2315.

[128] Sun, M.; Hong, C.-Y.; Pan, C. Y. A unique aliphatic tertiary amine chromophore: Fluorescence, polymer structure, and application in cell imaging. *J. Am. Chem. Soc.* **2012**, *134*, 20581–20584.

[129] Zhu, Q.; Qiu, F.; Zhu, B. S.; Zhu, X. Y. Hyperbranched polymers for bioimaging. *RSC Adv.* **2013**, *3*, 2071–2083.

[130] Hong, Y. N.; Lam, J. W. Y.; Tang, B. Z. Aggregation-induced emission: Phenomenon, mechanism and applications. *Chem. Commun.* **2009**, 4332–4353.

[131] Hong, Y. N.; Lam, J. W. Y.; Tang, B. Z. Aggregation-induced emission. *Chem. Soc. Rev.* **2011**, *40*, 5361–5388.

[132] Mirtchev, P.; Henderson, E. J.; Soheilnia, N.; Yip, C. M.; Ozin, G. A. Solution phase synthesis of carbon quantum dots as sensitizers for nanocrystalline TiO_2 solar cells. *J. Mater. Chem.* **2012**, *22*, 1265–1269.

[133] Gupta, V.; Chaudhary, N.; Srivastava, R.; Sharma, G. D.; Bhardwaj, R.; Chand, S. Luminscent graphene quantum dots for organic photovoltaic devices. *J. Am. Chem. Soc.* **2011**, *133*, 9960–9963.

[134] Zhang, X. Y.; Zhang, Y.; Wang, Y.; Kalytchuk, S.; Kershaw, S. V.; Wang, Y. H.; Wang, P.; Zhang, T. Q.; Zhao, Y.; Zhang, H. Z. et al. Color-switchable electroluminescence of carbon dot light-emitting diodes. *ACS Nano* **2013**, *7*, 11234–11241.

[135] Shen, J. H.; Zhu, Y. H.; Yang, X. L.; Zong, J.; Zhang, J. M.; Li, C. Z. One-pot hydrothermal synthesis of graphene quantum dots surface-passivated by polyethylene glycol and their photoelectric conversion under near-infrared light. *New J. Chem.* **2012**, *36*, 97–101.

[136] Liu, W.-W.; Feng, Y.-Q.; Yan, X.-B.; Chen, J.-T.; Xue, Q.-J. Superior micro-supercapacitors based on graphene quantum dots. *Adv. Funct. Mater.* **2013**, *23*, 4111–4122.

[137] Lin, Z.; Xue, W.; Chen, H.; Lin, J.-M. Peroxynitrous-acid-induced chemiluminescence of fluorescent carbon dots for nitrite sensing. *Anal.Chem.* **2011**, *83*, 8245–8251.

[138] Liu, J.-J.; Zhang, X.-L.; Cong, Z.-X.; Chen, Z.-T.; Yang, H.-H.; Chen, G.-N. Glutathione-functionalized graphene quantum dots as selective fluorescent probes for phosphate-containing metabolites. *Nanoscale* **2013**, *5*, 1810–1815.

[139] Li, X.; Zhu, S. J.; Xu, B.; Ma, K.; Zhang, J. H.; Yang, B.; Tian, W. J. Self-assembled graphene quantum dots induced by cytochrome c: A novel biosensor for trypsin with remarkable fluorescence enhancement. *Nanoscale* **2013**, *5*, 7776–7779.

[140] Tang, J.; Kong, B.; Wu, H.; Xu, M.; Wang, Y. C.; Wang, Y. L.; Zhao, D. Y.; Zheng, G. F. Carbon nanodots featuring efficient FRET for real-time monitoring of drug delivery and two-photon imaging. *Adv. Mater.* **2013**, *25*, 6569–6574.

[141] Markovic, Z. M.; Ristic, B. Z.; Arsikin, K. M.; Klisic, D. G.; Harhaji-Trajkovic, L. M.; Todorovic-Markovic, B. M.; Kepic, D. P.; Kravic-Stevovic, T. K.; Jovanovic, S. P.; Milenkovic, M. M. et al. Graphene quantum dots as autophagy-inducing photodynamic agents. *Biomaterials* **2012**, *33*, 7084–7092.

[142] Xie, Z.; Wang, F.; Liu, C.-Y. Organic-inorganic hybrid functional carbon dot gel glasses. *Adv. Mater.* **2012**, *24*, 1716–1721.

[143] Zhang, G. Y.; Zhang, H.; Zhang, X. R.; Zhu, S. J.; Zhang, L.; Meng, Q. N.; Wang, M. Y.; Li, Y. F.; Yang, B. Embedding graphene nanoparticles into poly(N,N′-dimethylacrylamine) to prepare transparent nanocomposite films with high refractive index. *J. Mater. Chem.* **2012**, *22*, 21218–21224.